OPTICAL SPECTROSCOPY OF ALEXANDRITE CRYSTALS

By

GUY DONALD GILLILAND

Bachelor of Science

Baylor University

Waco, Texas

1984

Submitted to the Faculty of the Graduate College
of the Oklahoma State University
in partial fulfillment of the requirements
for the Degree of
MASTER OF SCIENCE
May, 1986

OPTICAL SPECTROSCOPY OF ALEXANDRITE CRYSTALS

Thesis Approved:

Richard A. Burrell
Thesis Adviser

H L Scott

Bruce J Ackerson

Norman N Durham
Dean of the Graduate College

ACKNOWLEDGMENTS

I would like to express my thanks to all the people responsible for helping me during my studies at Oklahoma State University. Foremost among these is my thesis adviser, Dr. Richard C. Powell. I want to thank him for giving me the chance to work in his laboratory both as an undergraduate and graduate student, and for his advice and support. I would also like to thank the other members of my committee, Dr. Bruce J. Ackerson and Dr. Hugh L. Scott. I also wish to express my appreciation to Dr. William A. Sibley for his advice and assistance in my professional career. Special thanks go to my friend Dr. Jacek K. Tyminski for his patience in sharing his knowledge of the field with me, and helping to set up the mode-locked laser. Further, I wish to thank Mrs. Dee Behrens for her help in completing this thesis.

I would like to thank the two people who have made all of this possible, my parents, Dr. and Mrs. Donald C. Gilliland. I want to thank them for putting me through school and their constant love and support. My special thanks to my beautiful and patient wife, Marcy. She helped make all of the long hours endurable.

Financial support for my graduate studies was provided by the Graduate Fellowship Program of the Office of Naval Support. Financial support for this work was also provided by the U. S. Army Research Office (Durham, N.C.), Department of the Army and by the National Science Foundation under Grant No. DMR-82-16551.

TABLE OF CONTENTS

LIST OF TABLES

LIST OF FIGURES

Figure Page

CHAPTER I

INTRODUCTION

In recent years alexandrite ($BeAl_2O_4:Cr^{3+}$) has been shown to be an important solid-state laser material. Alexandrite is a mechanically strong and chemically stable material. Large, high-quality alexandrite crystals can be grown by a modified Czochralski method. The physical properties of the host material, chrysoberyl, enable this material to withstand high average power optical pumping. The importance of this material is due to its tunability. Alexandrite is only the third material in which Cr^{3+} has been reported to lase, and is one of a few solid-state laser materials shown to exhibit tunability, among them $Ni:MgF_2$, $Co^{2+}:MgF_2$, and $V^{2+}:MgF_2$ (1). However, alexandrite is the first of these materials to operate efficiently at room temperature and above. Its laser characteristics are very versatile; among them, its tunability from 700 to 818 nm, and its ability to be Q-switched. Alexandrite has fluorescent R-line emissions, from the ^2E states to the $^4A_2$ state, and a vibronic emission, concurrent emission or absorption of phonons with the electronic transition from $^4T_2$ to $^4A_2$, which appears as a broad band in the fluorescent spectra. These states are shown in the energy level diagram of Figure 1. The R-line emission was shown to lase in 1974, and subsequently the broadband emission was shown to lase in 1977 (1).

In alexandrite Cr^{3+} ions can exist in two crystallographically inequivalent octahedrally coordinated sites; one with mirror site C_s

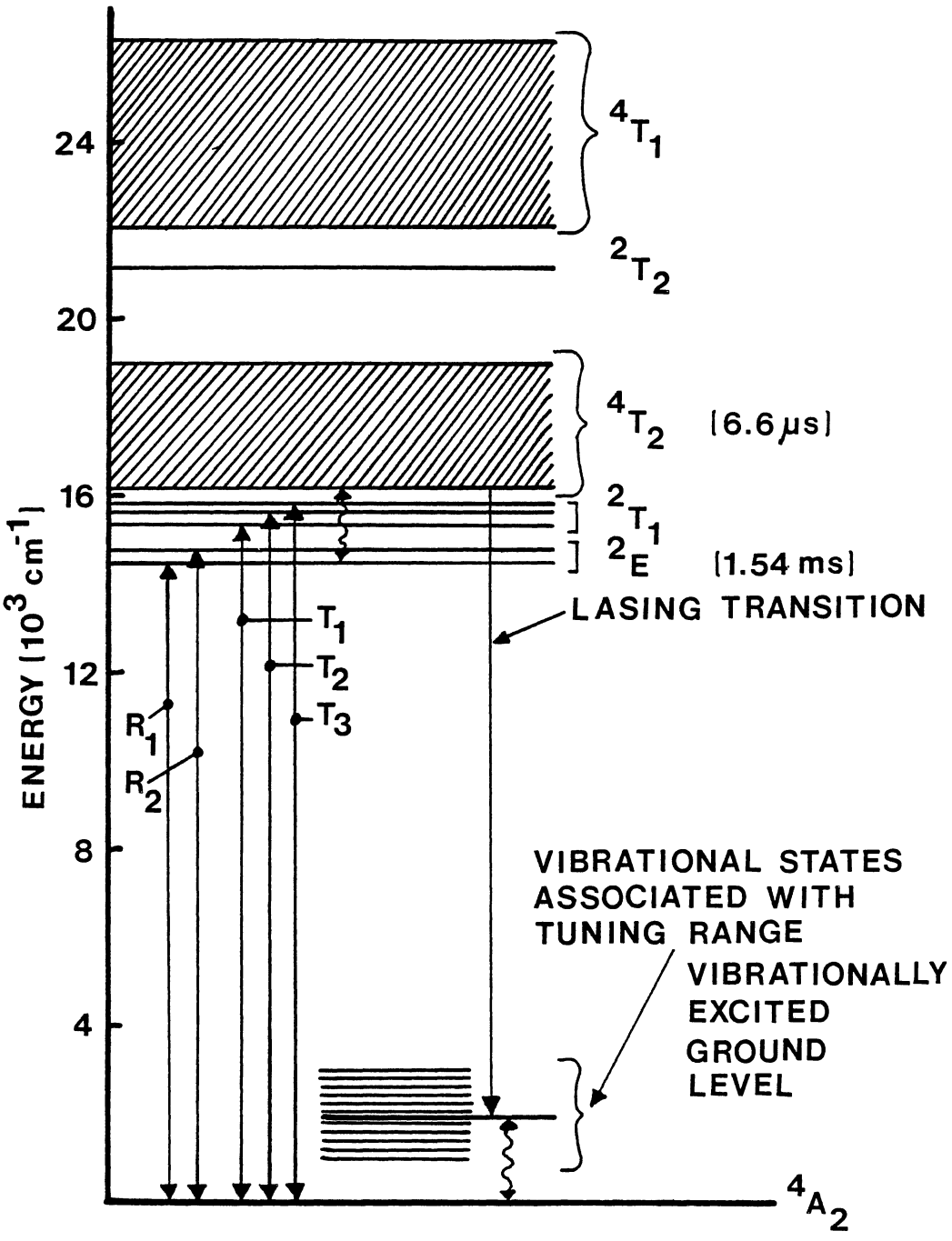

Figure 1. Energy Level Diagram for Mirror Site Cr^{3+} Ions in Alexandrite

symmetry and one with inversion site C_i symmetry. The lasing action occurs for the Cr^{3+} ions in the mirror sites and not the inversion sites. Because of energy transfer from the mirror site ions to the lower-energy inversion site ions (2), the spectroscopic properties of the inversion site ions are not totally irrelevant to the laser operation. The dynamical processes are also important to study, and the nonlinear optical characteristics of this material can give an understanding of these processes. The spectroscopic properties of alexandrite have been studied previously, but not much work has been done on the nonlinear optical properties (2,3).

The dynamical processes that occur are radiative and nonradiative transitions. These transitions are easily envisioned in terms of the energy level diagram shown in Figure 1. Excitation into the $^4T_1$ band will decay to the $^2T_2$, $^2T_1$, or ^2E states by fast nonradiative emission and the same processes occurs for $^2T_2$ to $^4T_2$, and $^4T_2$ to $^2T_1$ and ^2E. If the Cr^{3+} ions are excited into $^2T_1$, decay to ^2E is by multiphonon emission, while the same type of decay from ^2E to $^4A_2$ is negligible. Excitation into the ^2E energy level can result in two processes: a radiative decay to $^4A_2$, or excitation thermally to $^2T_1$ or $^4T_2$. Radiative transitions can occur between either $^2T_1$ or $^4T_2$ to $^4A_2$. Nonradiative transitions from $^4T_2$ to $^4A_2$ are also possible (4). In particular the ^2E and $^2T_1$ levels are in thermal equilibrium with the $^4T_2$ band and thus the nonradiative processes occurring between these states are important to the lasing action.

Summary of Thesis

In this study, nondegenerate four-wave mixing (FWM) is used to investigate the nonlinear optical properties of alexandrite. Data

include temperature dependence and write beam crossing angle dependence of the FWM scattering efficiency for the inversion site Cr^{3+} ions. The absolute scattering efficiency at 7.5^{o} was measured at temperatures ranging from 25 K to 300 K. A model is proposed to describe the scattering efficiency as a function of the angle between the write beams, and this model is found to give a good fit to the experimental data. From this model, the change in the real and imaginary parts of the complex index of refraction are calculated. The relative predominance of the two types of gratings that can be formed, dispersion or absorption, is then calculated. The phase coherence relaxation time is calculated, and this gives very important information concerning the nonradiative decay rate from $^{4}T_{2}$ to ^{2}E.

Vibronic, anti-Stokes excitation, and Raman spectra are presented. Group theoretical techniques are used to analyze the Raman spectra and assign a specific phonon symmetry to the peaks in the spectra. Data include the vibronic spectrum at $10^{o}K$, anti-Stokes excitation spectrum at room temperature, and Raman spectra of both alexandrite and undoped chrysoberyl at room temperature.

CHAPTER II

EXPERIMENTAL PROCEDURE

Samples

The sample investigated in this study was a cube of alexandrite, $BeAl_2O_4:Cr^{3+}$, with each edge measuring about 6 mm. It contained 0.0325 at. % Cr^{3+} ions and was obtained from Allied Corporation. For the Raman studies a sample of undoped chrysoberyl measuring 0.360 x 0.388 x 0.303 inches and also from Allied Corporation was used. Some of the spectroscopic, chemical, and mechanical, features of alexandrite have been reported previously (2,3). Alexandrite is trichroic. The different crystallographic axes can be distinguished by the different colors of the crystal when viewed through the different faces. This is shown in Figure 2.

Four-Wave Mixing Scattering Efficiency

The experimental setup for nondegenerate four-wave mixing (FWM) is shown schematically, Figure 3. The measurements reported here were done using a Spectra Physics model 164 Argon-Ion Laser as a source of excitation. The powers of the write beams were kept about the same by using a 50% beam splitter (BS). The write beams cross in the sample at an angle 2θ and their interference forms a sine-wave pattern which acts as an index of refraction grating. A chopper (CH) was used to

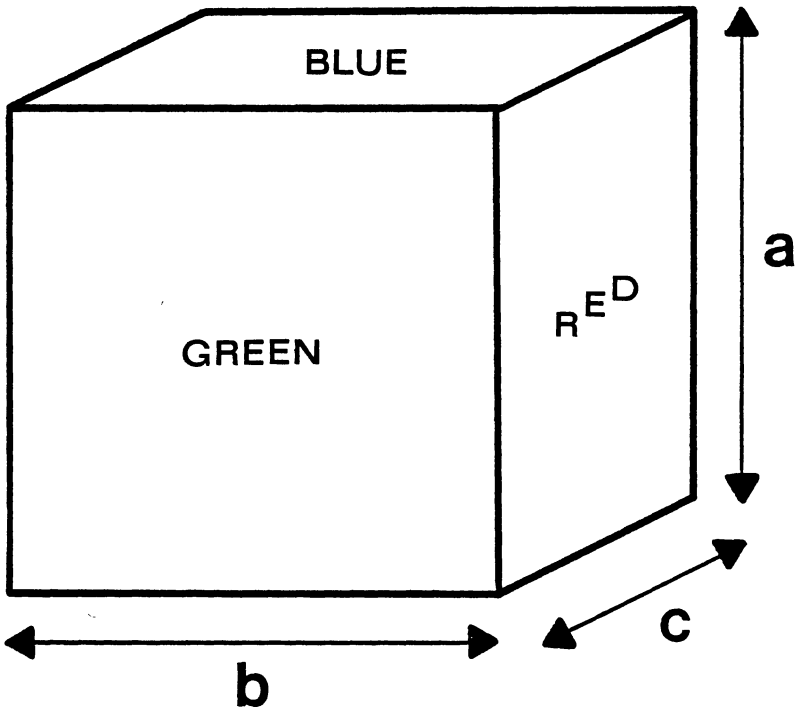

Figure 2. Orientation of Crystal Axes in Relation to the Colors of the Crystal Faces

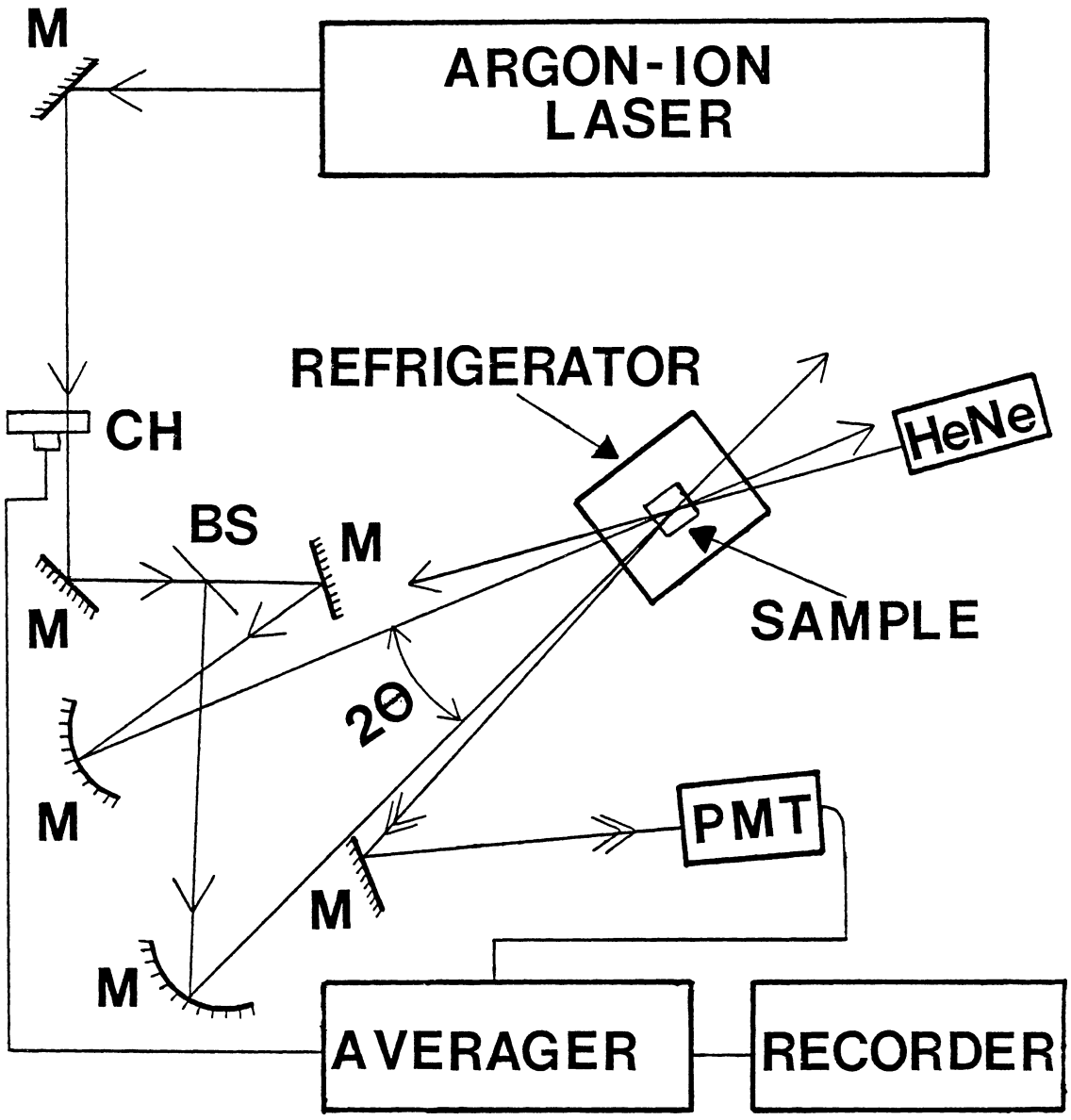

Figure 3. Experimental Apparatus for Four-Wave Mixing Scattering Efficiency and Grating Lifetime Measurements

turn off the write beams at a variable frequency for the grating lifetime measurements. The read beam enters the sample in a direction counterpropagating to the write beam E_1 and slightly offset so as to match the Bragg condition. The read beam is partially diffracted by the grating resulting in the signal beam leaving the sample in a direction slightly offset from the counterpropagating direction to write beam E_2 thus satisfying the Bragg diffraction condition (5), Figure 4. An EG&G Princeton Applied Research Model 4202 Signal Averager and a model PM 2254B Amperex photomultiplier tube were used for detection of the signal. The data were printed with a Houston Instruments Omniscribe Series D5000 strip chart recorder. A model 22C Cryodyne Cryocooler from CTI-Cryogenics was used for the low temperature work. The vibration isolation part of the cold head was model number 22 from Cryosystems Inc. A gold-iron constan thermocouple and a model ADP-E temperature controller from Air Products Inc. were used to determine and control the temperature of the sample. The absolute and relative scattering efficiencies were measured with this experimental setup at temperatures ranging from 25 K to room temperature.

Anti-Stokes Excitation Spectrum

The experimental setup for this experiment is shown in Figure 5. A Molectron UV-14 Nitrogen Laser and Dye Laser was used as the wavelength tunable source. It has a pulse width of approximately 10 ns and a variable repetition rate up to about 20 Hz. The dye for this laser was an Oxazine 720 Perchlorate dye obtained from Exciton Chemical Company. The dye was a 4.63×10^{-3} M solution of Ox720P in a solvent of 92% ethanol and 8% DMSO mixed 1:1 with a 5×10^{-3} M solution of Rhodamine

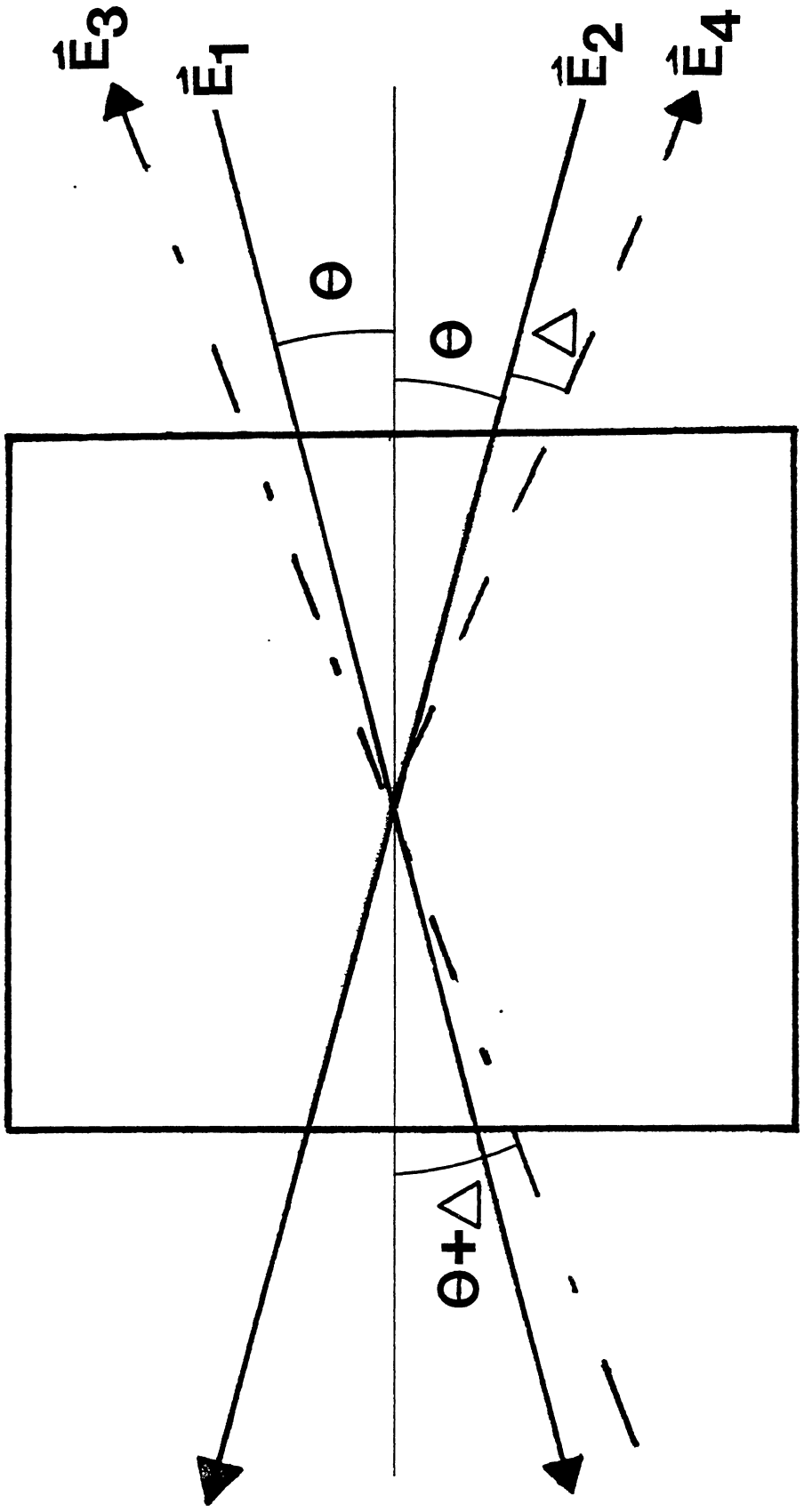

Figure 4. Geometry of the Laser Beams in Four-Wave Mixing

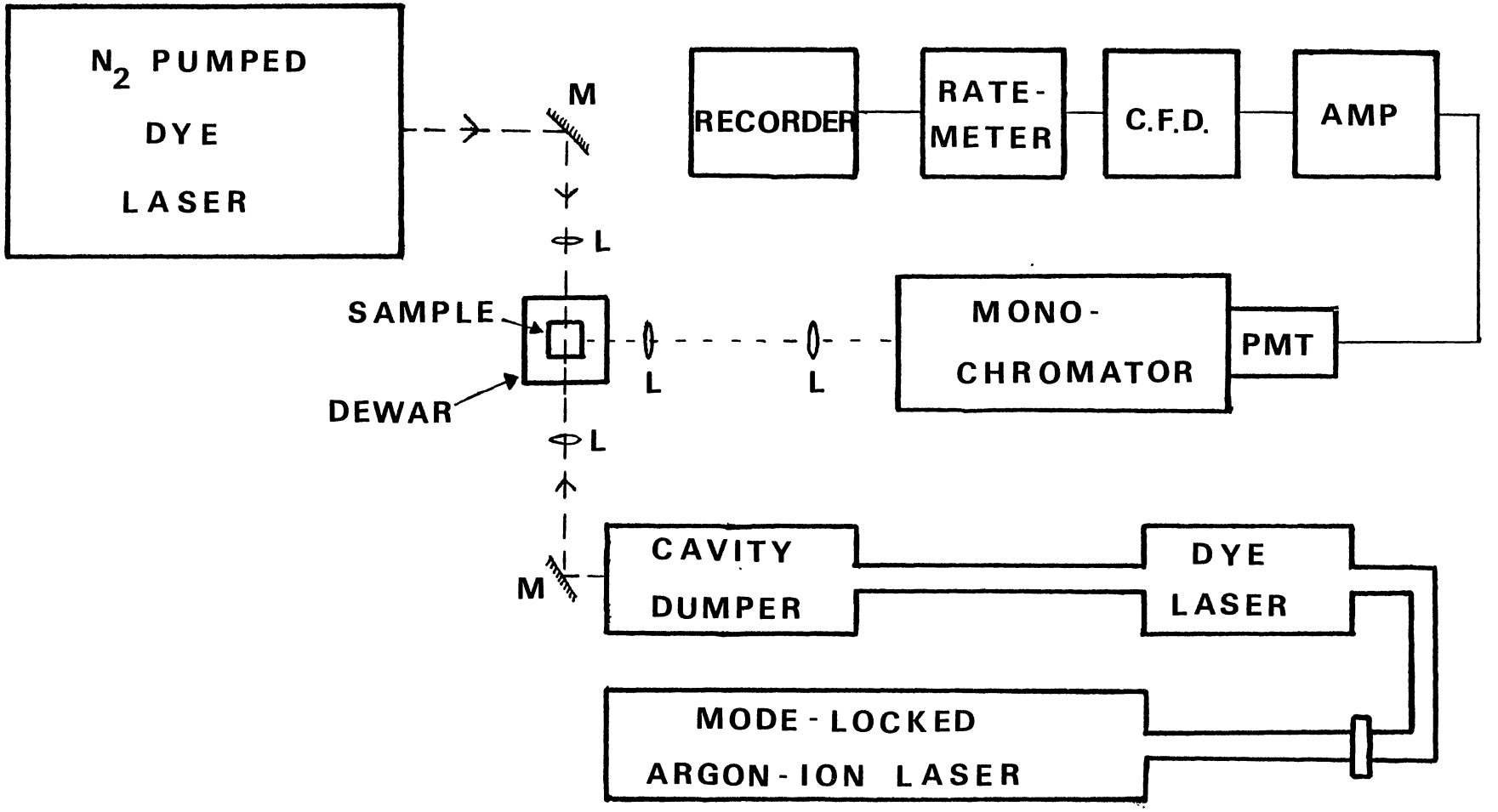

Figure 5. Experimental Apparatus for Anti-Stokes Excitation Spectra

610 in a 100% ethanol solvent. This dye lased in a wavelength range that was tunable from 6785Å down to 6650Å. The intensity of the dye laser was measured over this range and then used to calibrate the spectra. The other excitation source was a synchronously pumped cavity dumped mode-locked dye laser system. The argon-ion laser was a Spectra Physics Model 164. The mode-locker was a Spectra Physics Model 342A Ultra-Stable Mode-Locking System. The Cavity Dumper and Driver were Spectra Physics Model Numbers 344S and 454, respectively. The dye laser, with Rhodamine 6G Dye, had a pulse width of about 30 ps and a variable repetition rate from 400 Hz to 8 MHz. The experimental setup consisted of setting the repetition rate of the nitrogen laser at its maximum, 20 Hz and the mode-locked laser at a repetition rate of 8 KHz. The electric field of the N_2 Dye Laser was vertical and that of the mode-locked laser was horizontal. The alexandrite sample was oriented so that the b-axis was parallel to the electric field of the N_2 Dye Laser to get maximum absorption of this laser wavelength. The pulses coming from the two lasers were not synchronized. The beams from the lasers were aligned counterpropagating, and the fluorescence of the sample was detected at 90^{o} to the laser beam direction. A Pacific Instruments Model MP-1018B Monochromator was used to measure the wavelength. The photomultiplier tube was a Model R1547 from Hamamatsu Corp. The signal from the PMT was amplified in an EG&G Ortec Model 535 Quad Fast Amplifier (AMP). The signal was then sent to an Ortec Model 463 Constant Fraction Discriminator (CFD) in order to lower the baseline, and then to an Ortec Model 9349 Log/Lin Ratemeter in order to determine the intensity of fluorescence. The intensity of the R_1 and R_2 mirror site fluorescent lines was monitored as the N_2 Dye Laser wavelength was tuned

away from resonance with the R lines. This was done at room temperature and at liquid nitrogen temperature with the sample in a liquid nitrogen dewar. The fluorescence was then measured without the N_2 Dye Laser and only the mode-locked laser. This was subtracted from the combined excitation spectra and then the data was normalized adjusting for the intensity spectrum of the N_2 Dye Laser. All of the data were printed out on a Houston Instruments Omniscribe Series D5000 strip chart recorder.

Vibronic Spectrum

The source of excitation in this experiment was a Molectron UV-14 N_2 Laser with Dye Laser. The dye used was Rhodamine 6G. The sample was mounted in an Air Products Model DE202 refrigerator with a Model CS-202 compressor unit. A Spex 1 meter monochromotor and a RCA C31034 photomultiplier tube were used to analyze the fluorescence signal. The signal from the phototube was processed by an EG&G Princeton Applied Research Corp. Model 162 Boxcar Averager with a Model 165 gated integrator module. The spectrum was printed on the strip chart recorder. Careful attention was paid to scanning the wavelength slow enough so that the boxcar could be set to reduce as much noise as possible and the slits on the monochromator could be closed as far as possible in order to provide maximum resolution. The scanning speed of the monochromator was 5$\mathring{A}$ per minute for the spectra taken. The experimental arrangement is shown in Figure 6. The spectrum was measured with the sample at 10 K using the refrigerator mentioned earlier.

Raman Spectra

The Raman spectra were taken by Dr. John Bowen with a laser micro-Raman apparatus. The spectra were taken with the electric field of

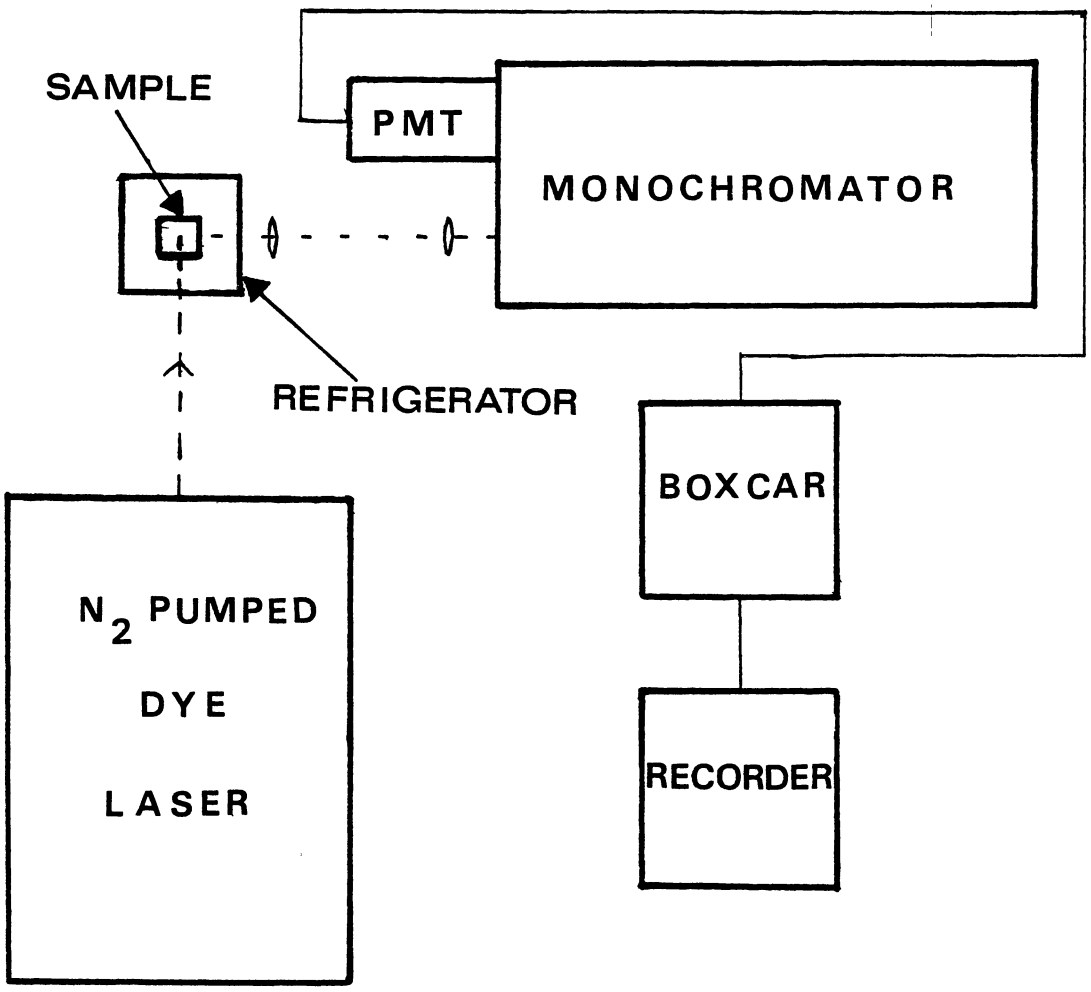

Figure 6. Experimental Apparatus for Low Temperature Fluoresence Spectra

the laser parallel to the different polarization axes shown in Figure 2. Both samples, the alexandrite and the undoped chrysoberyl, were given to Bowen for analysis in this equipment. In Chapter IV, these will be compared with the vibronic spectrum and anti-Stokes spectrum mentioned earlier.

CHAPTER III

FOUR-WAVE MIXING SCATTERING EFFICIENCY

Theory

The basis of the analysis done in this study is that a transient population grating is formed in the crystal and that the probe beam is scattered from this grating. The interference of the write beams in the interaction region forms a sinusoidal interference pattern and a similar distribution of Cr^{3+} ions in the excited states. This spatially varying excited-state population distribution behaves like a diffraction grating, due to the differences in the absolute value of the complex dielectric constant, n, of the material when the Cr^{3+} ions are in the ground or excited states. This complex dielectric constant can also be thought of in terms of the complex susceptibility or polarization (6) since

$$\varepsilon = 1 + 4\pi\chi \tag{1}$$

and

$$P = \chi E \tag{2}$$

In FWM the scattering efficiency of nonlinear media has a definite write beam angle dependence. A theory for scattering efficiency versus angle for photorefractive materials, such as lithium niobate, has been presented by Feinberg (7), but no such theory for scattering efficiency as a function of crossing angle exists for materials in which a

population grating is produced. This section of the study presents a model for the scattering efficiency as a function of write beam angle for such materials. A two level system was used as a model for the population grating. The density matrix formalism is needed since the exact state of the system is not known. The geometric configuration of the electric fields in the FWM apparatus is shown in Figure 4. The electric fields are all polarized in the same direction, parallel to the b-axis of the crystal in this study. The equations of motion for the elements of the density matrix, ρ, termed the master equations and written as $i\hbar\frac{d\rho}{dt} = [H,\rho]$, are obtainable from the total Hamiltonian of the system (8)

$$H = H_o + H_I + H_R \tag{3}$$

where

$$H_o = \begin{bmatrix} E_a & 0 \\ 0 & E_b \end{bmatrix} \tag{4}$$

are the zeroth-order energy eigenvalues of the ground and excited state, $|a\rangle$ and $|b\rangle$ respectively. The interaction Hamiltonian, H_I, can be written as

$$H_I = \begin{bmatrix} 0 & -\tilde{\mu}E(\vec{r},t) \\ -\tilde{\mu}E(\vec{r},t) & 0 \end{bmatrix} \tag{5}$$

where $\tilde{\mu}$ is the dipole moment, and $E(\vec{r},t)$ is the applied electric field. The ensemble average of the dipole moment of an atom in an electric field, $\langle\tilde{\mu}\rangle$, is given by

$$\langle\tilde{\mu}\rangle = \text{Trace}(\rho\tilde{\mu}) = \tilde{\mu}(\rho_{12} + \rho_{21}) \tag{6}$$

The relaxation part of the master equations can be dealt with in a

quasi-phenomenological manner. The elements of the density matrix decay to their thermal equilibrium values (designated by superscript e) in a certain characteristic time. The equilibrium values for the diagonal elements (ρ^e_{11} and ρ^e_{22}) are given by the Boltzmann factors. The relaxation time for the diagonal elements in a two level system is the same, τ, and is called the longitudinal relaxation time. The off-diagonal elements decay with a different relaxation time, T_2, called the transverse relaxation time. T_2 can be thought of as a phase coherence relaxation time since the off-diagonal elements are zero when the system is in equilibrium. The relaxation term in the total Hamiltonian returns the system to statistical equilibrium via collisions, spontaneous emission, etc. The relaxation part of the master equations become (8)

$$(i\hbar)^{-1} [H_R,\rho]_{11} = (\rho^e_{11} - \rho_{11})/\tau \tag{7a}$$

$$(i\hbar)^{-1} [H_R,\rho]_{22} = (\rho^e_{22} - \rho_{22})/\tau \tag{7b}$$

$$(i\hbar)^{-1} [H_R,\rho]_{12} = -\rho_{12}/T_2 \tag{7c}$$

These equations can be combined to give the total master equations for the two-level system (9):

$$\dot{\sigma}_{12} = i(\omega - \omega_{21})\sigma_{12} + i\Omega(\rho_{11} - \rho_{22}) - \sigma_{12}/T_2 \tag{8a}$$

$$\dot{\rho}_{11} - \dot{\rho}_{22} = 2i\Omega(\sigma_{21} - \sigma^*_{21}) - \frac{1}{\tau}[(\rho_{11} - \rho_{22}) - (\rho^e_{11} - \rho^e_{22})] \tag{8b}$$

where $\rho_{12} = \sigma_{12} e^{-i\omega t}$, $\Omega \equiv \frac{\tilde{\mu}E}{2\hbar}$ is the dipole moment precession frequency, $\omega_{21} \equiv \frac{1}{\hbar}(E_b - E_a)$ is the resonant frequency, and ω is the frequency of

the pump beams. These equations can be solved to give the polarization

$$P = N\langle\tilde{\mu}\rangle = \frac{\tilde{\mu}^2 \Delta N_o T_2 E}{\hbar}\left[\frac{\sin\omega t + (\omega_{21} - \omega)T_2\cos\omega t}{1 + (\omega - \omega_{21})^2 T_2^2 + 4\Omega^2 T_2 \tau}\right] \tag{9}$$

where N is the density of atoms, and ΔN_o is the average equilibrium density of the population difference between the ground and excited states, $\Delta N_o \equiv N(\rho_{11}^e - \rho_{22}^e)$. The real and imaginary parts of the electric susceptibility can be obtained from the polarization and can be combined to give the susceptibility (9)

$$\chi = \frac{\tilde{\mu}^2 \Delta N_o T_2}{\hbar}\left[\frac{T_2(\omega_{21} - \omega) - i}{1 + (\omega - \omega_{21})^2 T_2^2 + 4\Omega^2 T_2 \tau}\right] \tag{10}$$

Absorption, dispersion, FWM, and saturation are all contained in the susceptibility χ (10).

Now, the approximation can be made that the electric fields are plane waves (11)

$$\begin{aligned}
\vec{E}_1(\vec{r},t) &= \frac{1}{2}\vec{A}_1 e^{-i(\omega t - \vec{K}_1\cdot\vec{r})} + c.c. \\
\vec{E}_2(\vec{r},t) &= \frac{1}{2}\vec{A}_2 e^{-i(\omega t - \vec{K}_2\cdot\vec{r})} + c.c. \\
\vec{E}_3(\vec{r},t) &= \frac{1}{2}\vec{A}_3 e^{-i(\omega' t - \vec{K}_3\cdot\vec{r})} + c.c. \\
\vec{E}_4(\vec{r},t) &= \frac{1}{2}\vec{A}_4 e^{-i(\omega' t - \vec{K}_4\cdot\vec{r})} + c.c.
\end{aligned} \tag{11}$$

where c.c. denotes complex conjugation, $\vec{E}_1$ and $\vec{E}_2$ are the pump fields, $\vec{E}_3$ is the read field, and $\vec{E}_4$ is the scattered field. In nondegenerate FWM $\omega \neq \omega'$. Since the pump beams are approximately of the same intensity and the read field is more intense than the scattered field, the electric field can be written as the sum of a primary and a perturbative field.

$$E = E' + \Delta E \tag{12}$$

where $E' = E_1 + E_3$ and $\Delta E = E_2 + E_4$

The wave equation for these fields in this medium is (6)

$$\nabla^2 E = \frac{\mu}{c^2}\frac{\partial^2 E}{\partial t^2} + \frac{4\pi\mu}{c^2}\frac{\partial^2 P}{\partial t^2} \tag{13}$$

in cgs units.

Before substituting the polarization into the wave equation, it should be rewritten as (10)

$$P(E) = \chi(E')\left[1 + \delta^2\right]\left[1 + \delta^2 + \frac{2|A_1|^2}{|A_S|^2}\right] +$$

$$\chi(E')E'\left[1 - \left(\frac{4E'\Delta E^*}{|A_S|^2}\right)\left(1 + \delta^2 + \frac{2|A_1|^2}{|A_S|^2}\right)^{-1}\right] \tag{14}$$

where $\delta \equiv (\omega - \omega_{21})T_2$ is the detuning parameter, and $|A_S|^2 = 4|E_S|^2 = \frac{4\tilde{n}^2}{T_2\tau\tilde{\mu}^2}$. It is useful to define the complex index of refraction, n, and the complex index modulation, Δn, as

$$\Delta n^* = \frac{2A_1^2}{|A_S|^2}\left[\frac{\alpha_o(i + \delta)}{\left(1 + \delta^2 + \frac{|A_1|^2}{|A_S^2|}\right)^2}\right] \tag{15}$$

and

$$n = \frac{-i\alpha_o\left(i + \delta\right)\left(1 + \delta^2\right)}{\left[1 + \delta^2 + \frac{|A_1|^2}{|A_S^2|}\right]^2} \tag{16}$$

where $\alpha_o = \frac{\tilde{\mu}^2 \Delta N_o T_2}{\tilde{n}}$ is the line center small-signal field attenuation coefficient, and * denotes complex conjugation.

After substituting the polarization and the fields, using the slowly varying envelope approximation, ignoring the time dependence, equating like K-vector exponentials, noting that $|\vec{K}_1| = |\vec{K}_2|$, $|\vec{A}_1| = |\vec{A}_2|$., $|\vec{K}_3| = |\vec{K}_4|$, making the assumption appropriate for degenerate FWM that $\vec{K}_2 = -\vec{K}_4$ and appropriate for scattering from a grating, and using the geometry of Figure 4 to calculate the dot products in the fields, two coupled partial differential equations of complex variables are obtained.

$$\frac{\partial A_2}{\partial r}\left(\frac{1}{2r} - iK_1\cos\Theta\right) + \frac{\partial A_2}{\partial \Theta}\left(\frac{iK_1}{r}\sin\Theta\right) + A_2\left(\frac{\mu\omega^2}{2c^2} - \frac{1}{2}K_1^2 + \frac{2\pi\mu\omega^2 in}{c^2}\right) =$$

$$\frac{2\pi\mu}{c^2}\left(\frac{\Delta n^*}{2}\right)\left\{A_2\omega^2 + A_4^*\omega'^2\right\} \tag{17a}$$

$$\frac{\partial A_4}{\partial r}\left(\frac{1}{2r} + iK_3\cos(\Theta + \Delta)\right) - \frac{\partial A_4}{\partial \Theta}\left(\frac{iK_3}{r}\sin(\Theta + \Delta)\right) + A_4\left(\frac{\mu\omega'^2}{2c^2} -\right.$$

$$\left.\frac{1}{2}K_3^2 + \frac{2\pi\mu\omega'^2 in}{c^2}\right) = \frac{2\pi\mu}{c^2}\left(\frac{\Delta n^*}{2}\right)\left\{A_4\omega'^2 + A_2^*\omega^2\right\} \tag{17b}$$

Now assuming small beam depletion due to the small absorption coefficient, $\frac{\partial A_2}{\partial r} << 1$ and $\frac{\partial A_4}{\partial r} << 1$, these equations become

$$\frac{\partial A_2}{\partial \Theta}\left(\frac{iK_1}{r}\sin\Theta\right) + A_2\left(\frac{\mu\omega^2}{2c^2} - \frac{1}{2}K_1^2 + \frac{2\pi\mu\omega^2 in}{c^2} - \frac{\pi\omega^2\mu\Delta n^*}{c^2}\right) = \frac{\pi\omega'^2\mu}{c^2}(\Delta n)^* A_4^* \tag{18a}$$

$$\frac{\partial A_4}{\partial \Theta}\left(\frac{-iK_3}{r}\sin(\Theta + \Delta)\right) + A_4\left(\frac{\mu\omega'^2}{2c^2} - \frac{1}{2}K_3^2 + \frac{2\pi\mu\omega'^2 in}{c^2} - \frac{\pi\omega'^2\mu\Delta n^*}{c^2}\right) =$$

$$\frac{\pi\omega 2\mu}{c^2}(\Delta n)^* A_2^* \tag{18b}$$

Note that the assumption of no beam depletion, here, applies to the scattered beam and the write beam. The write beams are not depleted much,

but there is some absorption, and this is contained in the complex refractive index.

Equating the real and imaginary parts of the above equations gives four real coupled equations. Making the approximation that Δ, which is necessary to meet the Bragg condition in nondegenerate FWM (5), is not a function of θ, and changing variables to $\theta = \theta + \Delta$ in Equation 18b, the four coupled equations become

$$\frac{\partial A_2^i}{\partial \theta} = \left\{ \left[A_2^r D_1^r - A_2^i D_1^i - A_2^r D_2^r - A_2^i D_2^i \right] K_1 \csc\theta - \left[D_2^r A_4^r - D_2^i A_4^i \right] \frac{K_3^2}{K_1} \csc\theta \right\} \tag{19a}$$

$$\frac{\partial A_2^r}{\partial \theta} = \left\{ \left[-A_2^i D_1^r - A_2^r D_1^i + A_2^i D_2^r - A_2^r D_2^i \right] K_1 \csc\theta - \left[D_2^i A_4^r + D_2^r A_4^i \right] \frac{K_3^2}{K_1} \csc\theta \right\} \tag{19b}$$

$$\frac{\partial A_4^i}{\partial \theta} = \left\{ \left[-A_4^r D_1^r + A_4^i D_1^i + A_4^r D_2^r + A_4^i D_2^i \right] K_3 \csc\theta + \left[D_2^r A_2^r - D_2^i A_2^i \right] \frac{K_1^2}{K_3} \csc\theta \right\} \tag{19c}$$

$$\frac{\partial A_4^r}{\partial \theta} = \left\{ \left[A_4^i D_1^r + A_4^r D_1^i - A_4^i D_2^r + A_4^r D_2^i \right] K_3 \csc\theta + \left[D_2^r A_2^i + D_2^i A_2^r \right] \frac{K_1^2}{K_3} \csc\theta \right\} \tag{19d}$$

where $D_1 \simeq r(2\pi\mu i n)$, $D_2^* = r(\pi\mu\Delta n^*)$, and superscripts r and i denote real and imaginary, respectively. The parameter r is of the same dimension or smaller than the width of the interaction region. Equations 19 cannot be solved in closed form, but they can be solved numerically. A computer program was written to do this. A fourth order Runge-Kutta method for the four coupled equations was employed (12). The efficiency, defined as

$$\eta = \frac{|A_4|^2}{|A_3|^2} \quad , \tag{20}$$

was calculated at points 1/40th of a degree apart, typically, and the step-size was decreased until no effect was apparent in the values of η at different values of crossing angle. The step size used was approximately 1/200th of a degree. The resulting curve was smoothed so that the resulting scattering efficiency would not change unphysically fast as a function of θ, and then the curve was normalized. The computations were done on an IBM PC and the graphics software was ASYST from Macmillan Software Company. This numerical solution generated the curve presented in the experimental results section of this study and to be discussed in that section, Figure 7. A more complete derivation of the coupled Equations 19 is given in the appendix.

By adjusting the four variable parameters and computing the scattering efficiency curve, the effect of each parameter can be inferred. Several of these graphs are shown in Figures 8, 9, and 10. The real and imaginary parts of the two constants have the same effect on the theoretically computed curve. The effect of the modulation constant is to shift the peak of the curve to larger angles and to make the curve narrower as the refractive index modulation constant is increased. The scattering efficiency peaks near zero degree crossing angle for small modulation constants. The complex refractive index constant has a totally different effect on the theoretical curve. As the index constant is increased, real or imaginary part or both, the scattering efficiency increases at larger crossing angles. The shape of the scattering efficiency versus angle curve is thus indicative of the relative amount of nonlinearity present in the material, and whether the scattering is predominantly from an absorption or dispersion grating.

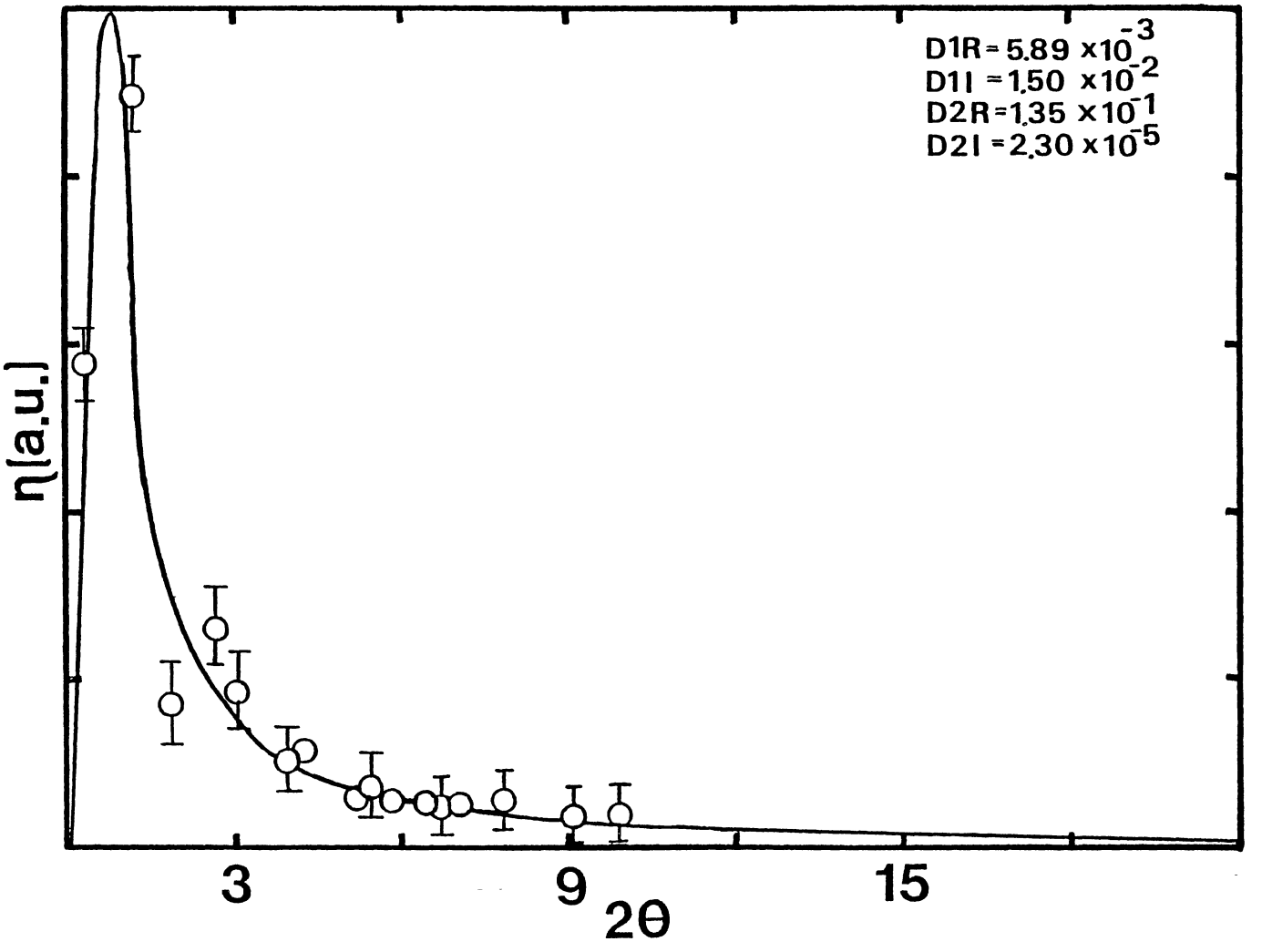

Figure 7. Four-Wave Mixing Scattering Efficiency and Theoretical Calculation (Solid line) with Variable Parameters

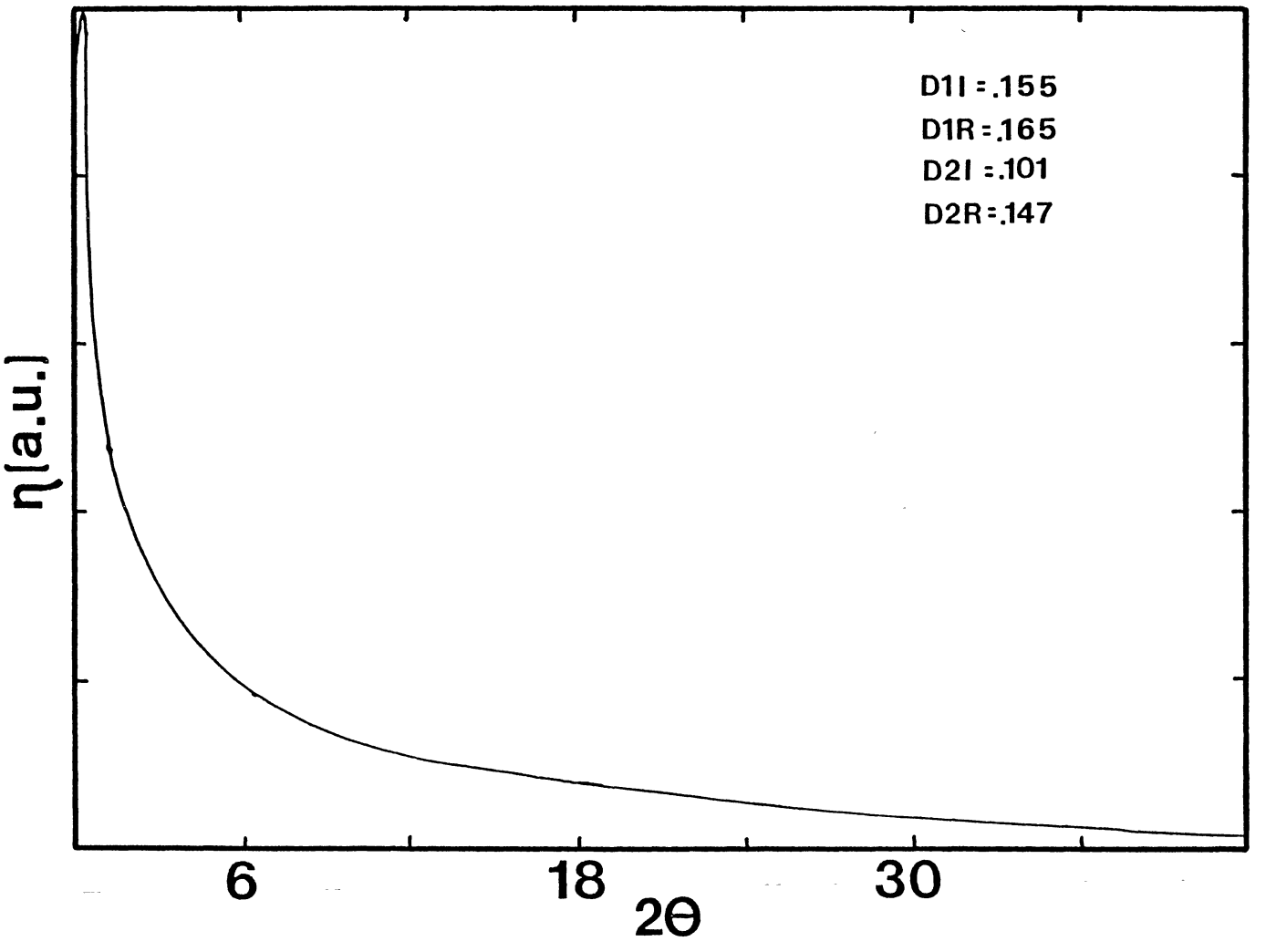

Figure 8. Theoretical Calculation of the Scattering Efficiency with Different Sets of Variable Parameters

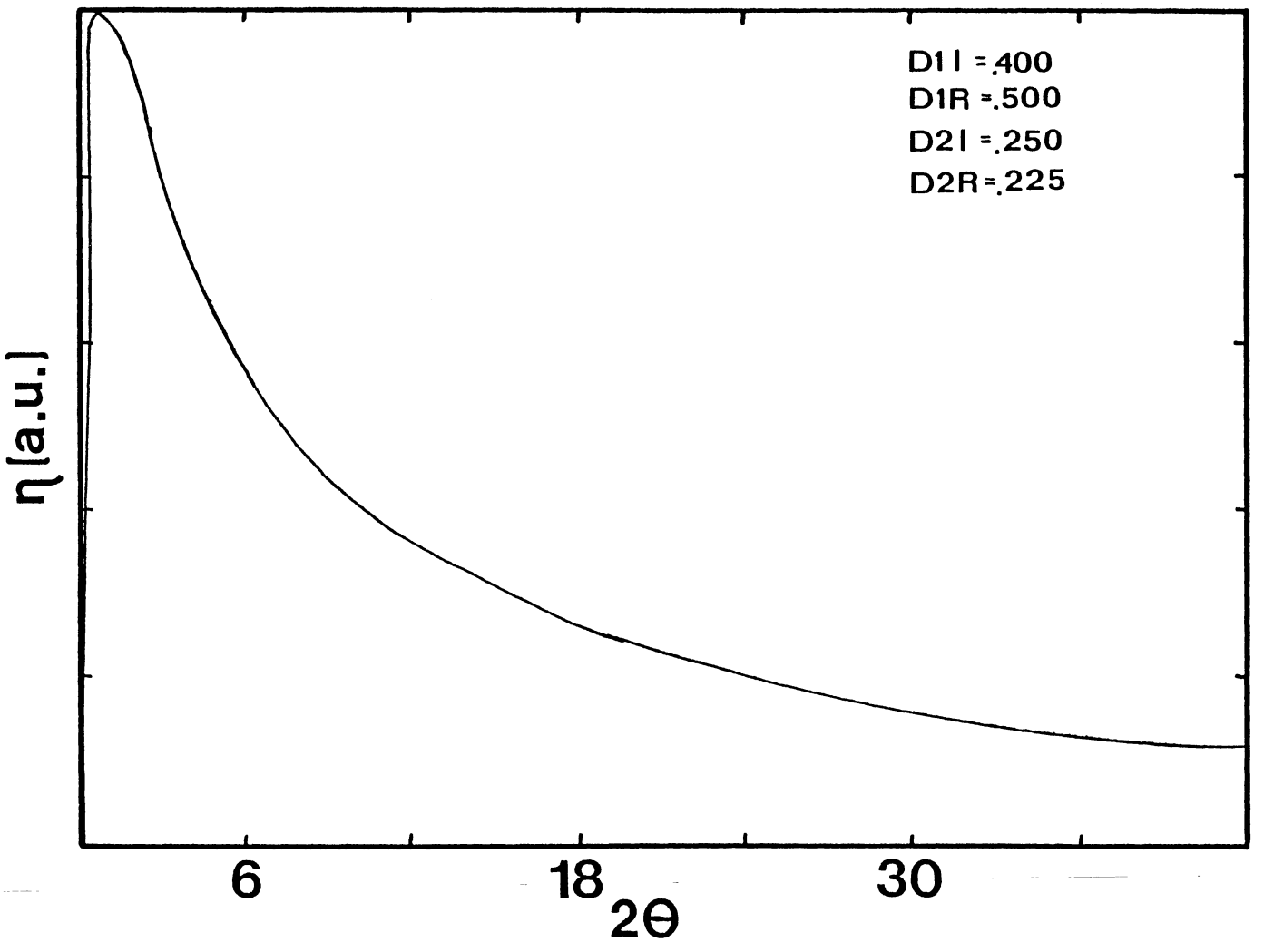

Figure 9. Theoretical Calculation of the Scattering Efficiency with Different Sets of Variable Parameters

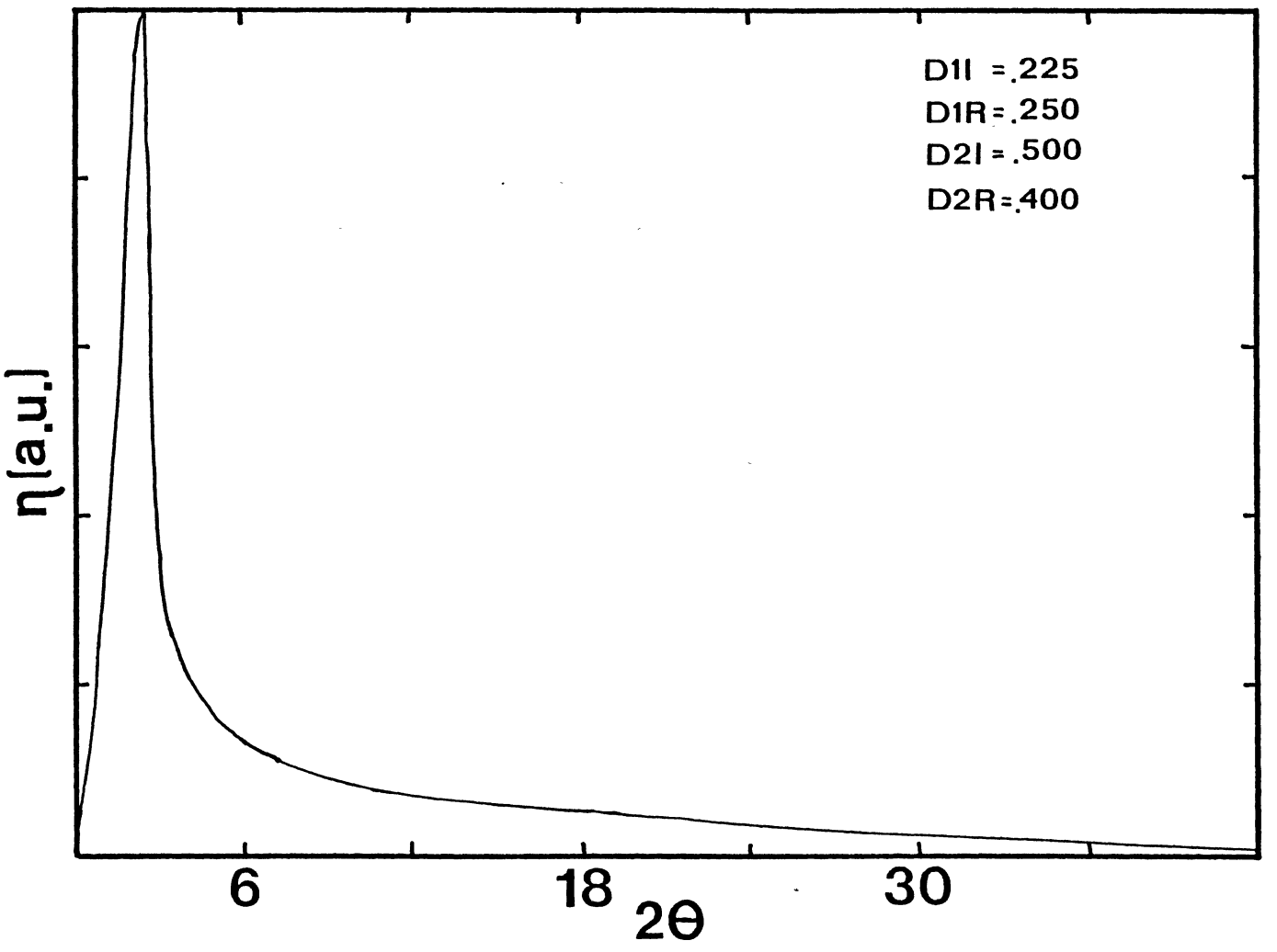

Figure 10. Theoretical Calculation of the Scattering Efficiency with Different Sets of Variable Parameters

One thing that should be noted is that the scattering efficiency is defined to be zero for zero write beam angle. This is physically reasonable since in this case there is no grating formed and thus nothing for the probe beam to scatter from, and it proved convenient since the numerical algorithm required a boundary condition (12). The computer generated plots all have a scattering efficiency of zero for a write beam angle of zero. This may not be visible in all of the plots due to the rapid increase in scattering efficiency at small angles. It is just this rapid change that makes the scattering efficiency very sensitive to vibrations and precise alignment of the write beams at small crossing angles. This is consistent with the results of Lawson, et al. (13).

Experimental Results

The scattering efficiency was measured for various angles and temperatures. The grating formed in the crystal was created by exciting the inversion site Cr^{3+} ions in the crystal. This was evident from the appearance of the R_{1i} lines in the fluorescent spectra when the excitation wavelength of 4880 Å was used, and the measured value of the grating lifetime. According to Powell, et al (2), the excitation wavelength, 4880 Å, excited the crystal in the valley between the strong absorption bands for the mirror sites, Figure 11, and in the peak of an absorption band for the inversion sites, Figure 12. The difference between the grating lifetimes measured, 30 ms, in this study and those measured in other studies (3), 24 ms, is due to differing concentrations of Cr^{3+} ions, the greater concentration having the smaller lifetime. The absolute scattering efficiency and angular dependence of the scattering

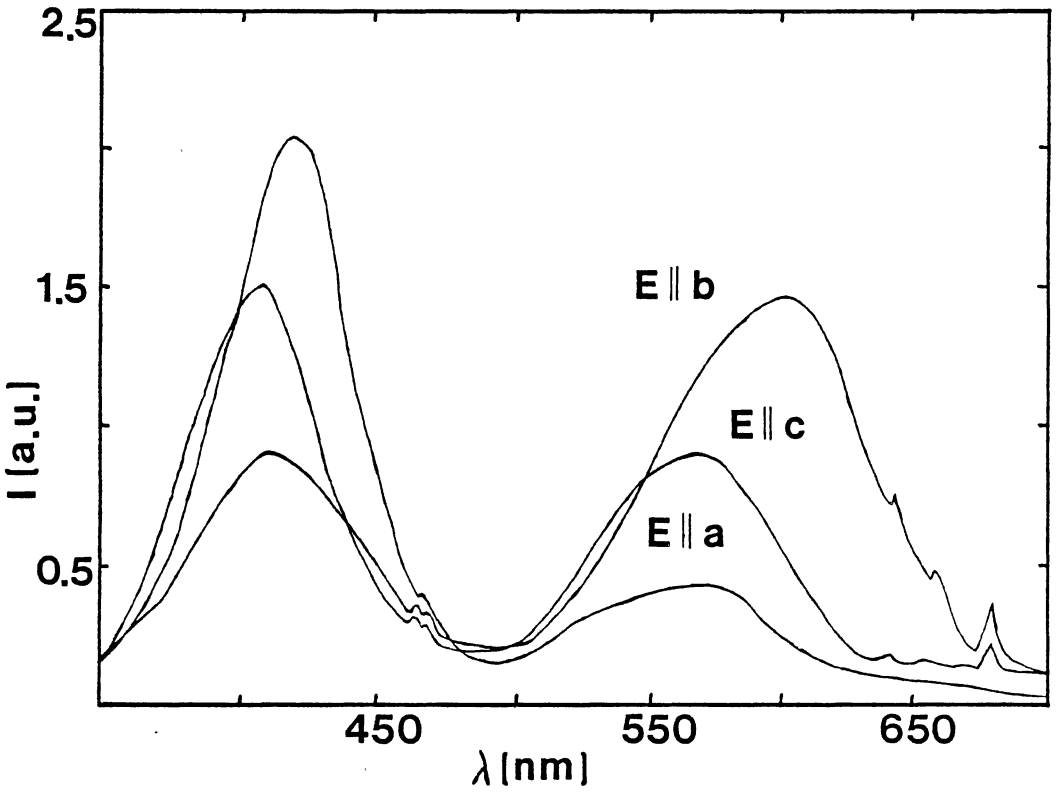

Figure 11. Room Temperature Absorption Spectra for Mirror Site Cr^{3+} Ions

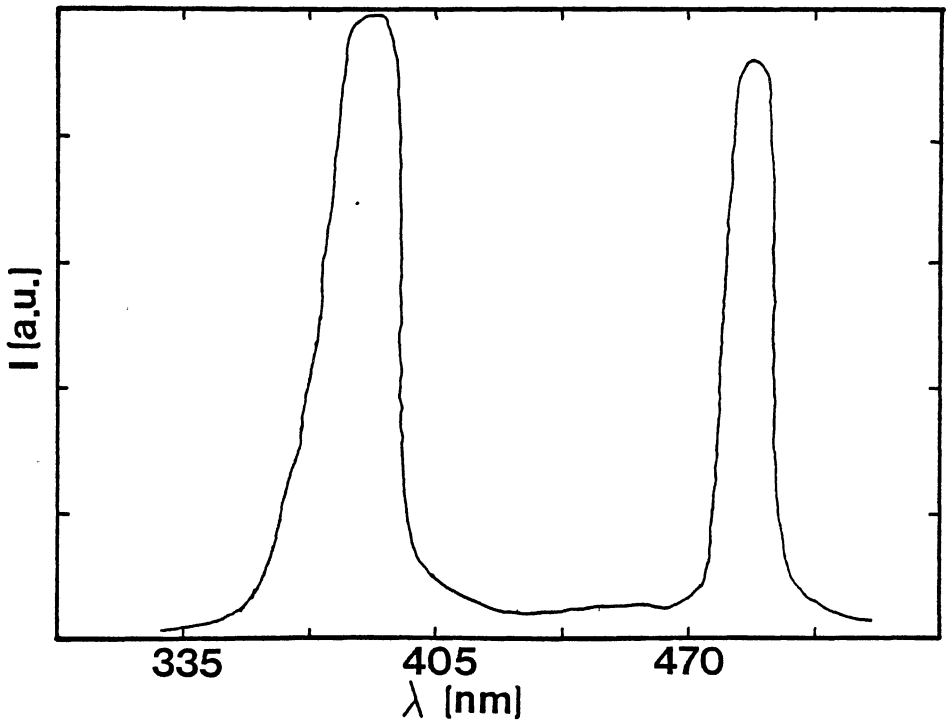

Figure 12. Room Temperature Excitation Spectrum for Inversion Site Cr^{3+} Ions

efficiency do not change with temperature. The absolute scattering efficiencies at various temperatures are shown in Figure 13. This is much smaller than the efficiency measured in photorefractive materials (7), but commensurate with that measured for materials in which excited state population gratings are formed (3), (14), (21). Thus, the results of this section of the study are applicable to ions in the inversion sites of the crystal.

The two-level model presented earlier is a reasonable approximation to the complex atomic processes occurring during excitation and relaxation of the atomic system. Support for this model comes from the shape of the angular dependence of the scattering efficiency curve. The theoretical curve from the model was fit to the experimental data at all temperatures collectively to give an estimate of the complex refractive index and complex modulation constant, Figure 7. The data was adjusted for the refractive index of the crystal before the fitting was done. There are several sources of error in the fitting. The experimental error in the experiment is not negligible as can be seen from the error bars in Figure 7. Also, the theoretical and experimental results were normalized, whereas in reality the experimental results may not have a maximum of 1.00 when properly fit with respect to the theory. A "scaling factor" was introduced to give better agreement between the data and theory, and every data point was multiplied by this same factor. Another complication arises in that the variable r appears in the expressions for the constants, and there is no data to give an estimate for r other than that it must be less than or equal to the size of the interaction region. For these reasons the ratios of the constants are the only attainable information. This problem can be somewhat circumvented to

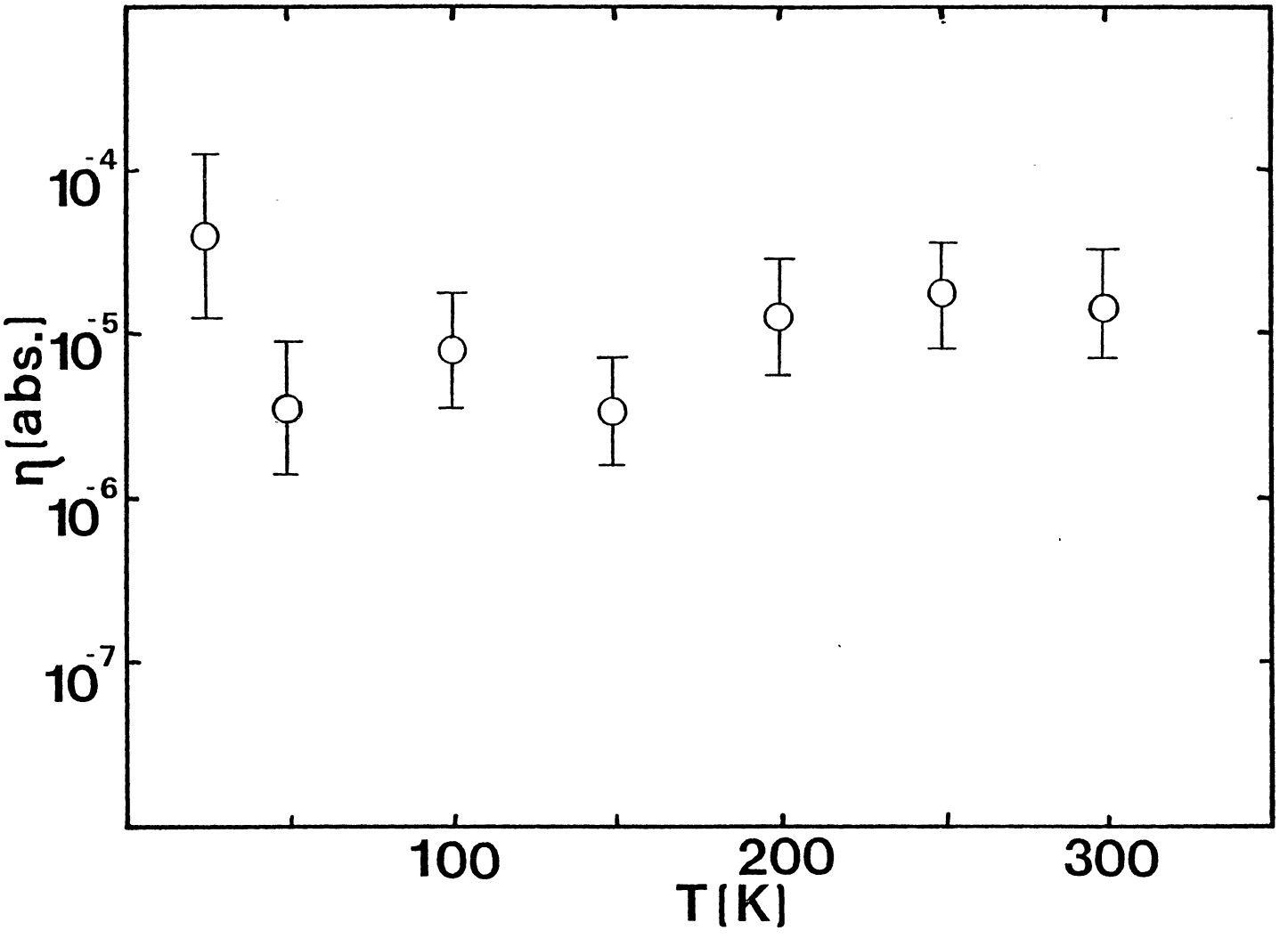

Figure 13. Four-Wave Mixing Absolute Scattering Efficiency at a Write Beam Crossing Angle of 7.5°

obtain an estimate for the constants by using the value of the previously measured absorption coefficient at the write beam wavelength. Another problem arises when attempting to fit the theory to the data, in that the numerical algorithm will produce the same curve for different sets of constants. It is thus necessary to have an estimate for the modulation constants to get accurate results.

Assuming the magnetic permeability of the material is approximately unity, $\mu \simeq 1$ the constants become

$$D_1^r = r(-2\pi\mu Im(n)) \simeq -2\pi r Im(n) \tag{21a}$$

$$D_1^i = r(2\pi\mu Re(n)) \simeq 2\pi r Re(n) \tag{21b}$$

$$D_2^r = r(\pi\mu Re(\Delta n)) \simeq \pi r Re(\Delta n) \tag{21c}$$

$$D_2^i = r(\pi\mu Im(\Delta n)) \simeq \pi r Im(\Delta n) \tag{21d}$$

Noting that the absorption coefficient for the write beam frequency, α, is defined as

$$\alpha \equiv 2\frac{\omega}{c} Im(n) \tag{22}$$

the modulation constants become

$$Re(\Delta n) \equiv \Delta\tilde{n} = \frac{\alpha c}{\omega}\frac{D_2^r}{D_1^r} \tag{23a}$$

$$Im(\Delta n) \equiv \frac{c\Delta\tilde{\alpha}}{2\omega} = \frac{\alpha c}{\omega}\frac{D_2^i}{D_1^r} \tag{23b}$$

These constants can be evaluated numerically if the constants from the "best-fit" curve, Figure 7, are used. With $\alpha = 0.36\ cm^{-1}$ (3)

$$\Delta\tilde{n} = 6.41 \times 10^{-5}$$

$$\Delta\tilde{\alpha} = 2.82 \times 10^{-3} \text{ cm}^{-1}$$

The values reported in (3) for these modulation constants are in good agreement with the values just calculated. The values reported by Powell are $\Delta\tilde{n} = 6.74 \times 10^{-5}$ and $\Delta\tilde{\alpha} = 2.62 \times 10^{-3}$ cm^{-1}. In the theoretical computation the magnitude of D_2^i, used to compute $\Delta\tilde{\alpha}$, was very small compared to the other constants and subject to the greatest amount of error because changes in this constant had little effect on the theoretical curve. On the other hand, the constant D_2^r used to calculate $\Delta\tilde{n}$ is fairly rigidly fixed since changes in D_2^r had an appreciable effect on the theoretical curve.

In order to determine whether the scattering mechanism is predominantly due to an absorption grating, the relatively simple formula for the scattering efficiency derived by Kogelnik is used (5)

$$\eta = e^{-2\alpha\Gamma}\left[\sinh^2\left(\frac{\Delta\tilde{\alpha}\Gamma}{2}\right) + \sin^2\left(\frac{\pi\Delta\tilde{n}\Gamma}{\lambda}\right)\right] \tag{24}$$

where $\Gamma = \frac{d}{\cos 2\Theta}$, d is the sample thickness, and λ is the wavelength of the write beams in the crystal. This equation was derived for the case of photorefractive materials where the physical mechanism is different than the present case. However, this equation can be employed to determine the relative importance of the macroscopic optical modulation constants $\Delta\tilde{\alpha}$ and $\Delta\tilde{n}$ since they appear explicitly in the equation. The scattering efficiency is greatest at small write beam crossing angles, 2Θ, and the sample thickness in this study was $d \simeq 0.8$ cm. Using this in Equation 24 and the values of $\Delta\tilde{\alpha}$ and $\Delta\tilde{n}$ calculated previously it is evident that the argument of sin and sinh are small. Thus these

functions may be expanded in a Taylor series and the higher order terms dropped. With these approximations the scattering efficiency becomes

$$\eta \simeq e^{-2\alpha\Gamma}\,\Gamma^2\left[\left(\frac{\Delta\tilde{\alpha}}{2}\right)^2 + \left(\frac{\pi\Delta\tilde{n}}{\lambda}\right)^2\right] \tag{25}$$

Thus, there are two terms that contribute to the scattering efficiency. One of the terms is due to an absorption grating, and the other is due to a dispersion grating. The relative strength of each of these in this study is

$$\frac{\eta(\Delta\tilde{\alpha})}{\eta(\Delta\tilde{n})} = \frac{(\Delta\tilde{\alpha})\lambda}{2\pi(\Delta\tilde{n})}^2 = 3.80 \times 10^{-8} \tag{26}$$

This result indicates that for this excitation wavelength the FWM signal is due almost totally to scattering from a dipersion grating. This is in agreement with the results obtained in (3).

It is now possible to calculate the phase coherence time, T_2, by using these results and Equation 15. The ratio of the real and imaginary parts of the modulation constant is related to phase coherence time by the relation

$$\frac{\mathrm{Re}(\Delta n)}{\mathrm{Im}(\Delta n)} = \frac{\Delta\tilde{n}}{\left(\frac{c}{2\omega}\,\Delta\tilde{\alpha}\right)} = \delta \equiv (\omega - \omega_{21})T_2 \,. \tag{27}$$

This can be solved for T_2.

$$T_2 = \frac{2\omega(\Delta\tilde{n})}{c(\Delta\tilde{\alpha})\,[\omega - \omega_{21}]} \tag{28}$$

It must be noted now that the two-level model presented in this study is only an approximation to the complex system of energy levels of Cr^{3+} ions in alexandrite. The excited state in the two level model is actually a combination of the $^4T_2$, $^2T_1$, and ^2E levels, and all of these levels are

in thermal equilibrium in the temperature range investigated. Therefore it is difficult to say what the exact resonant frequency, ω_{21}, of the system is. Absorption into the $^4T_2$ "pump band" results in fast relaxation to the ^2E metastable state. If the resonant frequency is chosen at the peak of this band, with $\lambda_{21} = 4790$ Å, the dephasing time becomes $T_2 = 80 \times 10^{-12}$ sec. The fact that there was no temperature dependence in the FWM measurements of $\Delta\tilde{n}$ and $\Delta\tilde{\alpha}$ indicates that strongly temperature dependent phonon scattering processes are not important. Thus it appears that the $^4T_2 - {}^2E$ radiationless relaxation does dominate the dephasing, which is an intrinsic property of the excited state in what has been defined as the excited state in the two-level model. This value for the dephasing time is only an estimate since this is only a rough model for the system. The parameters obtained from this work are summarized in Table I.

The modulation constant $\Delta\tilde{\alpha}$ can also be calculated from measurements of the ground and excited state absorption cross sections, σ_1 and σ_2, and the fluorescence decay time of the excited state, τ_{21}. The equation describing this relationship is (3)

$$\Delta\tilde{\alpha} = \frac{N_o I_o \sigma_1 (\sigma_2 - \sigma_1)}{2I_o\sigma_1 + (h\nu)\tau_{21}^{-1}} \tag{29}$$

where N_o is the concentration of active ions, I_o is the energy density of the write beams with photon energy $h\nu$. It is difficult to theoretically calculate the contribution to the FWM signal due to dispersion changes, $\Delta\tilde{n}$, because this involves the sum over all possible transitions of the Cr^{3+} ions in both the ground and metastable states. The technique presented in this study provides a method of calculating both the

TABLE I

SUMMARY OF RESULTS OF FWM MEASUREMENTS ON ALEXANDRITE

PARAMETER	CALCULATED VALUES
η	$\sim 10^{-5}$ (at $2\theta = 7.5^{o}$)
α (cm^{-1})	0.36
$\Delta\tilde{n}$	6.41×10^{-5}
$\Delta\tilde{\alpha}$ (cm^{-1})	2.82×10^{-3}
$\frac{\eta(\Delta\tilde{\alpha})}{\eta(\Delta n)}$	3.80×10^{-8}
T_2(ps)	80 ± 5

absorption and dispersion contributions to the FWM signal. However, the calculation of $\Delta\tilde{n}$ is more accurate than that of $\Delta\tilde{\alpha}$ since the grating is predominantly a dispersion grating.

CHAPTER IV

RAMAN, VIBRONIC, AND ANTI-STOKES EXCITATION SPECTRA

Theory

The host crystal of alexandrite, chrysoberyl, has a hexagonal close-packed structure. It is a member of the olivine family of crystals with four molecules per unit cell in an orthorhombic structure of space group P_{nma} (1),(2). As mentioned earlier the Al^{3+} ions are octahedrally coordinated by the oxygen ions in two inequivalent crystallographic sites, mirror sites with C_s symmetry and inversion sites with C_i symmetry. The Cr^{3+} ions enter the crystal substitutionally for the Al^{3+} ions, with the majority occupying the mirror sites. The six oxygen ligands produce a crystal field with O_h point-group symmetry. This symmetry is slightly distorted to C_s and C_i symmetry for the mirror and inversion sites, respectively. The electronic configuration of the Cr^{3+} dopant ions is (Argon)$3d^3$ and the O_h crystal field splits the free-ion wave functions into crystal-field wave functions with t^3- or t^2e- electron configurations. The spin multiplicities of the wave functions are either quartet or doublet (15),(16). This information is a necessary background to the point-group theoretical analysis to follow.

Raman spectroscopy is one of the main methods of obtaining information about a crystal's vibration frequencies. The Raman process corresponds to a mechanism by which incident light of frequency ω_i

interacts with the crystal to create or destroy lattice vibrations (phonons), and the energy gained or lost by the lattice is compensated for by a decrease (Stokes line) or increase (anti-Stokes line) of the frequency, ω_s, of the scattered light (17). The first-order Raman effect, in which a single phonon is created or destroyed, is the process analyzed in this study. Group theory predicts that only lattice vibrations of certain types of symmetry, depending on the crystal symmetry, give rise to Raman scattering.

The intensity of the scattered radiation is proportional to the electric moment of the crystal squared, $|M|^2$, where

$$M_\rho = \sum_\sigma \alpha_{\rho\sigma} E_\sigma \ , \tag{30}$$

$\vec{E}$ is the electric field of the incident light, and $\alpha_{\rho\sigma}$ is the polarizability tensor of the electrons in the crystal. The electrons in the crystal are the intermediary through which the incident radiation interacts with the lattice vibrations. According to Loudon (18) the electronic polarizability can be expanded in a power series of $\vec{r}$

$$\alpha_{\rho\sigma} = \alpha_{\rho\sigma}^{(0)} + \sum_\mu \alpha_{\rho\sigma,\mu} r_\mu + \sum_{\mu\nu} \alpha_{\rho\sigma,\mu\nu} r_\mu r_\nu + \ldots \tag{31}$$

where

$$\alpha_{\rho\sigma,\mu} = \left(\frac{\partial \alpha_{\rho\sigma}}{\partial r_\mu} \right)_{r = 0}$$

$$\alpha_{\rho\sigma,\mu\nu} = \left(\frac{\partial^2 \alpha_{\rho\sigma}}{\partial r_\mu \partial r_\nu} \right)_{r = 0} .$$

The first-order Raman scattering process is due to the term linear in r. When the assumption is made that the phonon frequency can be neglected in comparison to the frequency of the incident light, the polarizability

tensor can be related to the Raman tensor

$$\alpha_{\rho\sigma,\mu} = \frac{-e^2}{m^2 \omega_i^2 \hbar^2 d} R^{\mu}_{\sigma\rho} (-\omega_i, \omega_i, 0) \tag{32}$$

where d is the lattice constant, and m is the mass of the electron. This means that R is a symmetric tensor since the polarizability is symmetric. The subscripts on R refer to the polarization directions of the incident and scattered photons, and the superscript is the direction of polarization of the phonon.

The selection rules for the Raman-active phonons can be determined from group theory. A phonon can be Raman-active if and only if the irreducible representation which represents the normal mode (phonon) is the same as one of the irreducible representations which occurs in the reduction of the representation of the polarizability tensor (16). According to Wilson, et al (19) the components of the polarizability tensor transform in the same way as quadratic functions of the Cartesian coordinates (x^2, y^2, z^2, xy, xz, yz). When impurity ions (Cr^{3+}) are present in the crystal the translational invariance of the crystal is destroyed and phonons of all wave vectors can be active in first-order Raman scattering. Because of the Cr^{3+} ions present in the crystal the irreducible representations that must be considered are not those of the space group of the crystal, but are the irreducible representations of the crystallographic point group.

The character table for O_h point-group symmetry is given in Table II. The normal modes for this type of symmetry are given by

TABLE II

CHARACTER TABLE FOR O_h SYMMETRY

O_h	E	$6C_4$	$3C_2$	$6C_2'$	$8C_3$	I	$6S_4$	$3\sigma_h$	$6\sigma_h'$	$8S_6$	
A_{1g}	1	1	1	1	1	1	1	1	1	1	$x^2+y^2+z^2$
A_{1u}	1	1	1	1	1	-1	-1	-1	-1	-1	
A_{2g}	1	-1	1	-1	1	1	-1	-1	-1	1	
A_{2u}	1	-1	1	-1	1	-1	1	-1	1	-1	
E_g	2	0	2	0	-1	2	0	2	0	-1	$(2z^2-x^2-y^2, x^2-y^2)$
E_u	2	0	2	0	-1	-2	0	-2	0	1	
T_{1g}	3	1	-1	-1	0	3	1	-1	-1	0	(Lx,Ly,Lz)
T_{1u}	3	1	-1	-1	0	-3	-1	1	1	0	(x,y,z)
T_{2g}	3	-1	-1	1	0	3	-1	-1	1	0	(xy,yz,zx)
T_{2u}	3	-1	-1	1	0	-3	1	1	-1	0	

Normal Modes $\Gamma_v = A_{1g} + E_g + 2T_{1u} + T_{2g} + T_{2u}$

Raman Active A_{1g} E_g T_{2g}

Infrared Active T_{1u}

Inactive T_{2u}

$$\Gamma_v = A_{1g} + E_g + 2T_{1u} + T_{2g} + T_{2u}$$

with the following selection rules

Raman Active : A_{1g}, E_g, T_{2g}

Infrared Active: T_{1u}

Inactive : T_{2u}

The A_{1g} mode is a "breathing" mode and the E_g and T_{2g} modes are "stretching" and "twisting" modes. One interesting point to note is that no normal mode is both Raman and Infrared active. This is due to the exclusion rule which applies only to crystals with a center of symmetry (16).

In alexandrite the point-group symmetry of the Cr^{3+} ions is distorted slightly from O_h to C_s or C_i symmetry. Thus it is necessary to find the Raman-active modes in a lower site symmetry. If the symmetry is lowered to D_{2h}, which is the factor group of O_h and is still just an approximation to the actual site symmetry, then the Raman-active modes can be found from the correlation table between O_h and D_{2h} symmetry, Table III. The Raman-active modes can also be found in the character table for D_{2h} point-group symmetry, Table III. There are four Raman-active normal mode symmetries: A_{1g}, B_{1g}, B_{2g}, and B_{3g}, but there are more than just four frequencies of phonon possible. This is because there are four molecules per unit cell, which means there should be 84 vibrational modes. Table IV shows the Raman tensors of the Raman-active modes. The different modes should be distinguishable by polarization selection rules due to the off-diagonal elements and the presence of six

TABLE III

CHARACTER TABLE FOR D_{2h} SYMMETRY AND CORRELATION TABLE BETWEEN O_h AND D_{2h} SYMMETRY

D_{2h}	E	$C_2(z)$	$C_2(y)$	$C_2(x)$	i	$\sigma(xy)$	$\sigma(xz)$	$\sigma(yz)$	
A_g	1	1	1	1	1	1	1	1	(x^2, y^2, z^2)
B_{1g}	1	1	-1	-1	1	1	-1	-1	(L_z, xy)
B_{2g}	1	-1	1	-1	1	-1	1	-1	(L_y, xz)
B_{3g}	1	-1	-1	1	1	-1	-1	1	(L_x, yz)
A_u	1	1	1	1	-1	-1	-1	-1	
B_{1u}	1	1	-1	-1	-1	-1	1	1	z
B_{2u}	1	-1	1	-1	-1	1	-1	1	y
B_{3u}	1	-1	-1	1	-1	1	1	-1	x

$\Gamma_v = 11A_g + 7B_{1g} + 11B_{2g} + 7B_{3g} + 10A_u + 14\,B_{1u} + 10B_{2u} + 14B_{3u}$

O_h	D_{2h}
A_{1g}	A_g
A_{2g}	A_g
E_g	$2A_g$
T_{1g}	$B_{1g} + B_{2g} + B_{3g}$
T_{2g}	$B_{1g} + B_{2g} + B_{3g}$
A_{1u}	A_u
A_{2u}	A_u
E_u	$2A_u$
T_{1u}	$B_{1u} + B_{2u} + B_{3u}$
T_{2u}	$B_{1u} + B_{2u} + B_{3u}$

TABLE IV

RAMAN TENSORS FOR THE FOUR RAMAN-ACTIVE MODES IN D_{2h} SYMMETRY

A_g	$\begin{bmatrix} a & 0 & 0 \\ 0 & b & 0 \\ 0 & 0 & c \end{bmatrix}$
B_{1g}	$\begin{bmatrix} 0 & d & 0 \\ d & 0 & 0 \\ 0 & 0 & 0 \end{bmatrix}$
B_{2g}	$\begin{bmatrix} 0 & 0 & e \\ 0 & 0 & 0 \\ e & 0 & 0 \end{bmatrix}$
B_{3g}	$\begin{bmatrix} 0 & 0 & 0 \\ 0 & 0 & f \\ 0 & f & 0 \end{bmatrix}$

independent Raman tensor components: $R_{xx} = a$, $R_{yy} = b$, $R_{zz} = c$, $R_{xy} = d$, $R_{xz} = e$, and $R_{yz} = f$. If the incident and scattered photons have polarizations in the directions of the unit vectors $\hat{e}_i$ and $\hat{e}_s$, respectively, then the scattering efficiency is (18)

$$S = A\left[\sum_{\rho,\sigma = x,y,z} e_i^{\sigma} R_{\sigma\rho} e_s^{\rho}\right]^2 \qquad (33)$$

where A is a constant, e_i^{σ} and e_s^{ρ} are components of the unit vectors along the principal axes, σ and ρ, of the crystal. Equation 33 is the origin of the polarization selection rule.

The geometry of the Raman scattering process is shown in Figure 14. The incident and scattered light are fixed at right-angles to each other and the crystal axes are at an angle ϕ to the direction of the K-vectors (in this study $\phi = 0$).

Experimental Results

The Raman spectra taken with the Laser micro-Raman by Bowen were taken with polarized incident light. The scattered light was not analyzed through a polarizer. The notation used is as follows:

x - direction ———> c - axis

y - direction ———> a - axis

z - direction ———> b - axis

The first letter in the incident face designation refers to the axis parallel to the polarized electric field. The Raman spectrum for laser light incident on the BC face of the alexandrite crystal is shown in Figure 15. These peaks are shown in Table V along with the mode assignments based on the D_{2h} point-group symmetry (20). Also shown in

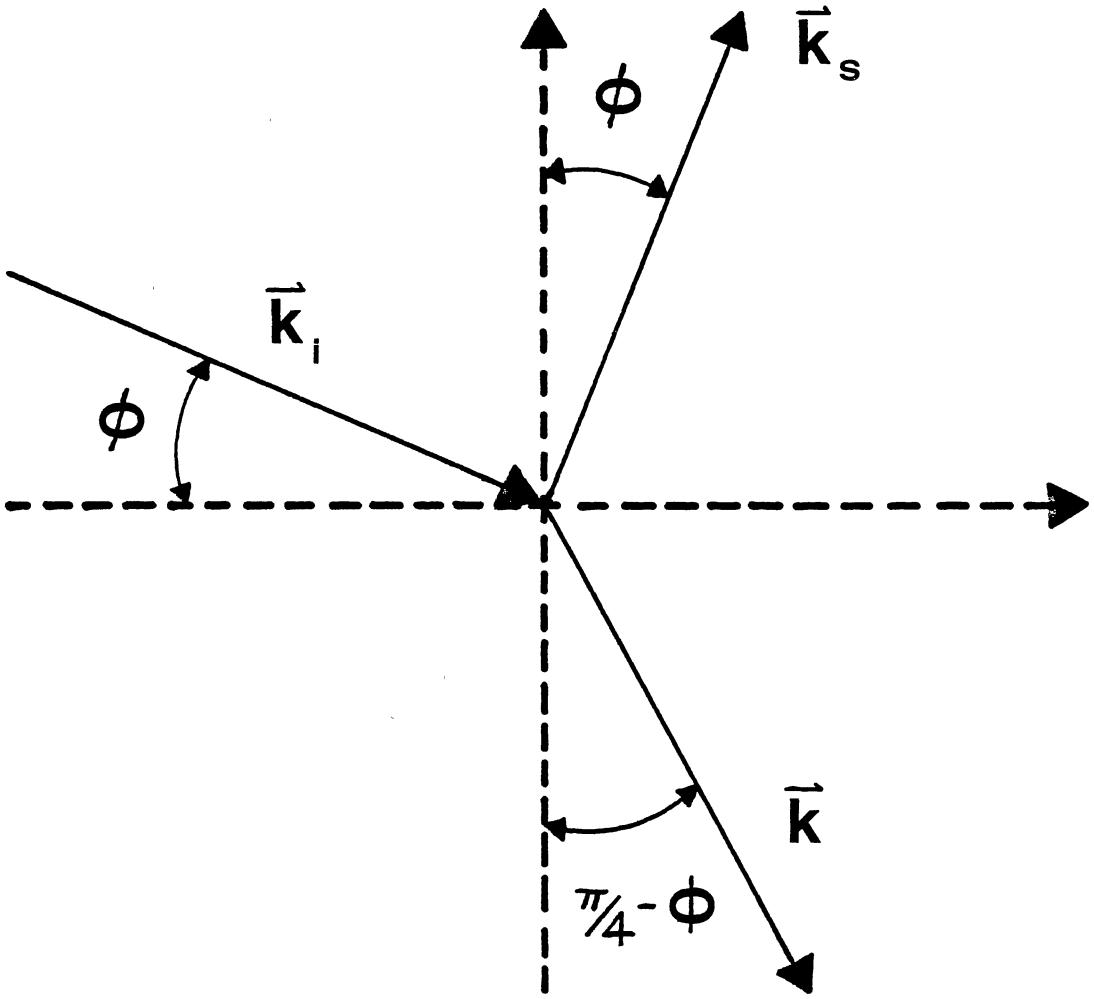

Figure 14. Geometry of Raman Scattering for Laser Light of Wave Vector $\vec{k}_i$ Incident at an Angle ϕ to the Crystal Axis, Scattered Light of Wave Vector $\vec{k}_s$, and Phonon Wave Vector $\vec{k}$ (Crystal Axes are Shown with Dashed Lines)

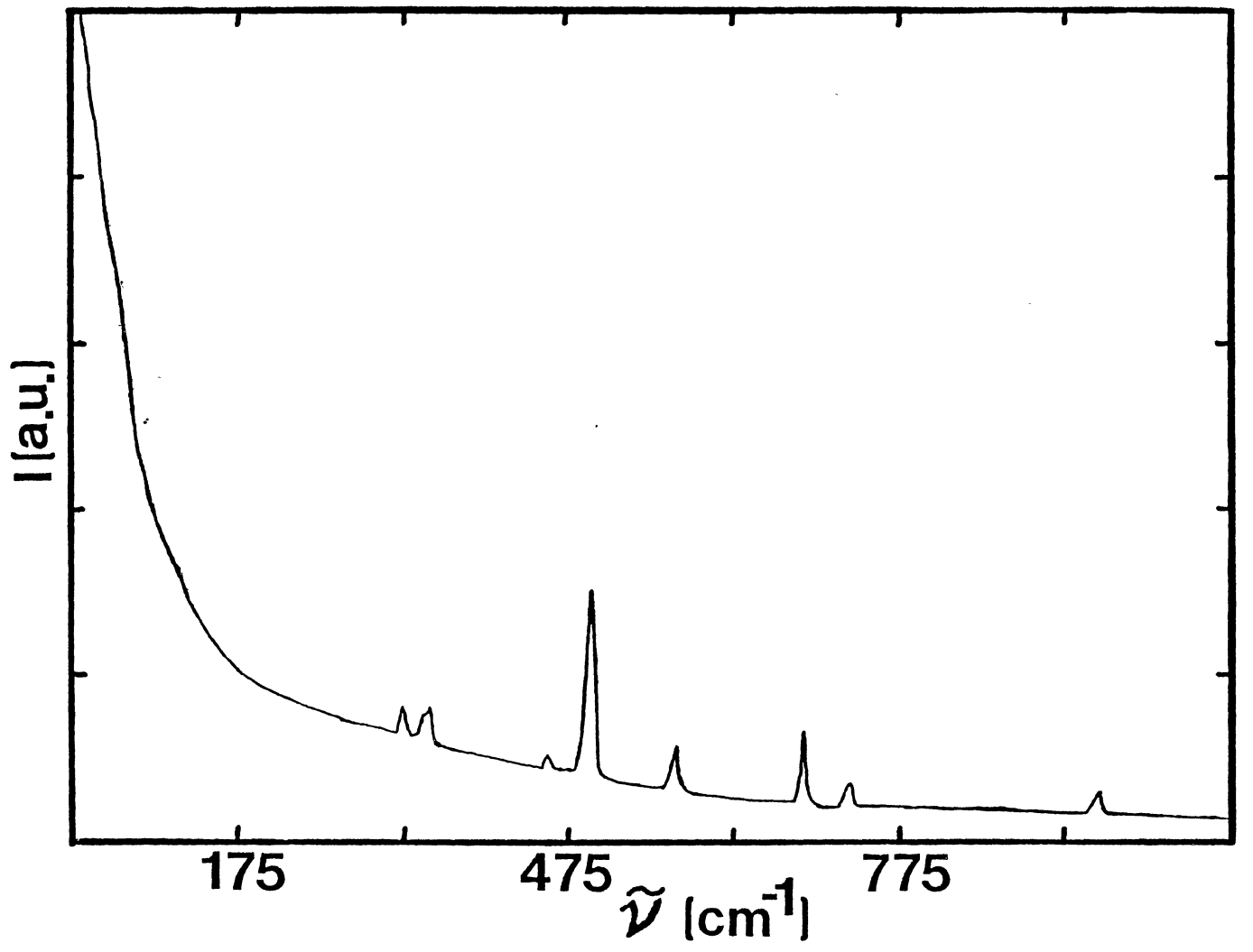

Figure 15. Entire Raman Spectrum for Light Incident on the BC Face of Alexandrite Crystal

TABLE V

PEAKS OF LOW TEMPERATURE EMISSION SPECTRUM, RAMAN SPECTRA OF ALEXANDRITE AND CHRYSOBERYL, AND MODE ASSIGNMENTS FOR BC ORIENTATION OF CRYSTAL

Vibronic (cm^{-1})	Alexandrite (cm^{-1})	Chrysoberyl (cm^{-1})	Mode Assignment
41			
62			**
75			
246	240	242	**
257			
276			
315			
	326		
352	358	356	B_{2g}
378			
392			B_{1g}
410			B_{2g}
	443	440	
455			A_g
459			
469			A_g
473			B_{3g}
477			
481	482	482	
490			B_{1g}
501			
510			B_{2g}
520	524	524	
534			B_{2g}

TABLE V (Continued)

Vibronic(cm^{-1})	Alexandrite(cm^{-1})	Chrysoberyl(cm^{-1})	Mode Assignment
560			B_{3g}
570	569	569	
586			
600			
610			
630			A_g
660			
680	683	680	
700			A_g
	749	749	
773			A_g
	782	782	
816			B_{1g}
	938	938	

Table V are the peaks in the Raman spectrum of the chrysoberyl sample. Figure 16 shows the fluorescence spectrum (vibronic) of alexandrite at 10 K. The peaks in this spectrum are also shown in Table V. The peaks in the anti-Stokes spectrum, marked with **, are also shown in Table V. It should be noted that the anti-Stokes spectrum did not have a resolution as good as the vibronic spectrum. The vibronic and anti-Stokes excitation spectra show several low frequency peaks. These could possibly be pair lines due to interactions of Cr^{3+} ions with each other.

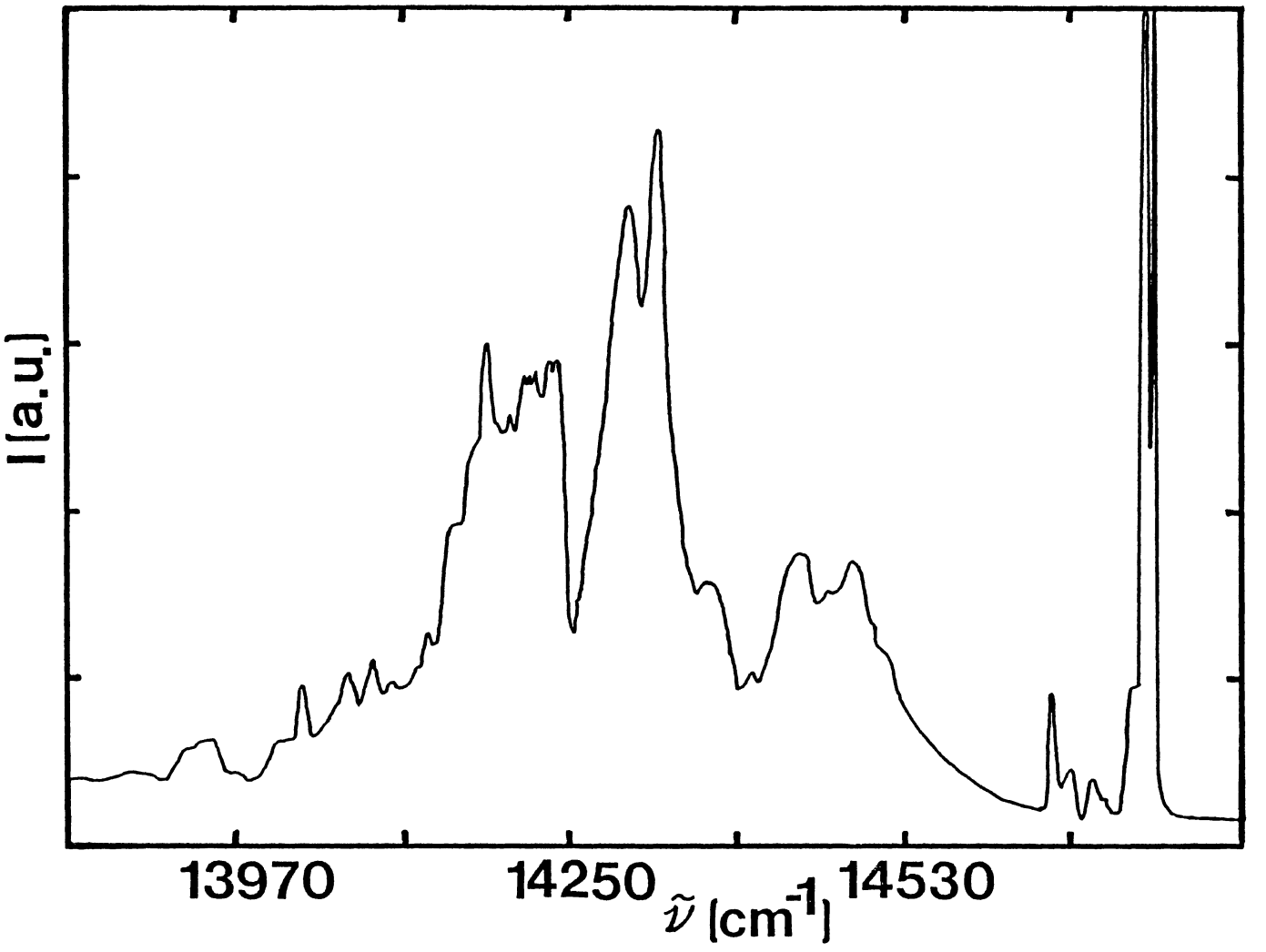

Figure 16. Fluorescence Spectrum at 10 K (Vibronic Spectrum) after 579.1 nm Excitation with R Lines at 14,720 cm^{-1}

CHAPTER V

SUMMARY AND CONCLUSIONS

In summary, the use of nondegenerate four-wave mixing in alexandrite has provided new information about the nonlinear optical properties and the excited-state dynamics of this system. The Raman spectra, anti-Stokes excitation spectrum, and vibronic spectrum provide information about the specific phonons present in alexandrite.

The two-level model presented in this study was shown to explain the write beam crossing angle dependence of the scattering efficiency, and from this model the optical modulation constants were calculated. These calculations also show that the FWM signal is predominantly due to scattering from a dispersion grating. There are several assumptions and limitations of the model used in this study that should be restated:

1. The atomic system under consideration is a two-level system.

2. The grating formed in the crystal due to the interference of the write beams creates an excited-state population distribution which behaves like a diffraction grating, due to the differences in the absolute value of the complex dielectric constant between the ground and excited states.

3. The electric fields are plane waves.

4. In nondegenerate FWM, K-vector conservation is similar to K-vector conservation in degenerate FWM.

5. The intensities of the two write beams are the same, and the intensities of the read and scattered beams are less than to the intensities of the write beams.

6. The intensity of the scattered beam is much less than the intensity of the read beam, i.e. the absolute scattering efficiency is small.

7. The slowly varying envelope approximation is used for the electric fields.

8. There is no beam depletion at the read beam wavelength, and only small depletion of the write beams.

9. The FWM scattering efficiency is defined to be zero for a write beam crossing angle of zero.

In fitting the theory to the data it is necessary to use the absorption coefficient at the write beam wavelength, measured by the standard spectroscopic techniques, in order to calculate the modulation constants $\Delta\tilde{n}$ and $\Delta\tilde{\alpha}$. It is also helpful to have an estimate of $\Delta\tilde{\alpha}$ because there are several sets of values which will fit the data. Therefore, the technique presented in this study is complementary to the calculation of Equation 29.

The calculation of the dephasing time, T_2, from Equation 28 provides very important information concerning the dynamics of the atomic system. In alexandrite T_2 can be interpreted as the nonradiative decay lifetime from the $^4T_2$ state to the ^2E state. This is one of the first reported measurements of this parameter. Therefore the model presented in this study provides a method of calculating these dephasing times which are on the picosecond time regime. The interpretation of T_2 as given here should be more accurate for systems that more closely resemble the two level system used in this model.

The Raman, Vibronic, and anti-Stokes data were presented in Table V. A point-group theoretical analysis by Weiyi, et. al. (20) was used to identify the specific phonon symmetry of the peaks. The low frequency lines present may be pair lines due to the interaction of Cr^{3+} ions, but there is no conclusive evidence for this as yet.

There is much more work to be done in the two areas researched in this study. A more detailed analysis and identification of the various peaks in the Raman and vibronic spectra of alexandrite should be done. Identification of these lattice vibrations is important because the optical transitions of the inversion site Cr^{3+} ions are forbidden, and the coupling between these phonons and the electronic states can increase the strength of these transitions. The FWM scattering efficiency should be measured in other crystals such as ruby, and then the modulation constants calculated. The dephasing time should be calculated and compared to alexandrite in order to have a better understanding of exactly what the dephasing time means. A temperature dependence of the FWM scattering efficiency should be measured in these crystals and the modulation constants and dephasing time calculated. This may provide information concerning the dynamics of the nonradiative decay processes occurring in the atomic system.

A SELECTED BIBLIOGRAPHY

1. Walling, J. C., O. G. Peterson, H. P. Jenssen, R. C. Morris, and E. W. O'Dell, IEEE J. Quantum Electronics QE-16, 1302 (1980).

2. Powell, R. C., L. Xi, X. Gang, G. J. Quarles, and J. C. Walling, Phys. Rev. B. 32, 2788 (1985).

3. Ghazzawi, A. M., J. K. Tyminski, R. C. Powell, and J. C. Walling, Phys. Rev. B 30, 7182 (1984).

4. Fonger, W. H. and C. W. Struck, Phys. Rev. B 11, 3251 (1975).

5. Kogelnik, H., Bell System Tech. J. 48, 2909 (1969).

6. Jackson, J. D., "Classical Electrodynamics" (Wiley, New York, 1975).

7. Feinberg, J., in "Optical Phase Conjugation," edited by R. A. Fisher (Academic Press, New York, 1983).

8. Levenson, M. D., "Introduction to Nonlinear Laser Spectroscopy," (Academic Press, New York, 1982).

9. Yariv, A., "Quantum Electronics" (Wiley, New York, 1975).

10. Abrams, R. L. and R. C. Lind, Optics Letters 2, 94 (1978).

11. Yariv, A. and D. M. Pepper, Optics Letters 1, 16 (1977).

12. Conte, S. D. and C. de Boor, "Elementary Numerical Analysis," (McGraw-Hill, New York, 1980).

13. Lawson, C. M., R. C. Powell, and W. K. Zwicker, Phys. Rev. B 26, 4836 (1982).

14. Tyminski, J. K., R. C. Powell, and W. K. Zwicker, Phys. Rev. B 29, 6074 (1984).

15. DiBartolo, B., "Optical Interactions in Solids," (Wiley, New York, 1968).

16. Cotton, F. A., "Chemical Applications of Group Theory," (Wiley, New York, 1963).

17. DiBartolo, B. and R. C. Powell, "Phonons and Resonances in Solids," (Wiley, New York, 1976).

18. Loudon, R., Advances in Physics 43, 423 (1964).

19. Wilson, E. B., J. C. Decius, and P. C. Cross, "Molecular Vibrations," (Academic Press, New York, 1982).

20. Weiyi, J., Z. Qingerong, S. Yusheng, W. Yanyun, Y. Zhenyl, H. Shouan, Z. Hetian, and L. Lilang, Kexue Tongbao 30-4, 452 (1985).

21. Liao, P. F. and D. M. Bloom, Optics Letters 3, 4 (1978).

APPENDIX

The model used here to describe the scattering efficiency's dependence on the angle between the write beams in nondegenerate FWM, see Figure 4, is a two level system for the atomic medium. Following Yariv and Abram's development to derive the polarization of the medium (1) (19). The Hamiltonian for the system is

$$H = H_o + H'$$

where H_o is the Hamiltonian in the absence of the electric fields. The exact state of the system is not known so the density matrix formalism must be used. The equation of motion is

$$i\hbar \frac{d\rho}{dt} = [H, \rho] \ . \qquad \text{(A1)}$$

The polarization is

$$P = N\langle\tilde{\mu}\rangle = N\text{Trace}(\rho\tilde{\mu}) \qquad \text{(A2)}$$

where $\langle\tilde{\mu}\rangle$ is the ensemble average of the atomic dipole moment of the atom that is induced by the fields. The time dependence of $e^{-i\omega t}$ assumed by Yariv (19) is a valid approximation since the amplitudes of the read and signal beams is small compared to the write beams the difference in frequency between the write beams and the read beam can be neglected. Hence, ω will refer to the pump beam frequency, Yariv includes collisional effects which tend to return the system to its statistical equilibrium condition. The final result for the

polarization with symbols as defined in Equations (5-10) is

$$P = \frac{\tilde{\mu}^2 \Delta N_o T_2}{\hbar} E \left[\frac{\sin\omega t + (\omega_{21} - \omega) T_2 \cos\omega t}{1 + 4\Omega^2 \tau T_2 + T_2^2 (\omega - \omega_{21})^2} \right] \tag{A3}$$

and the electronic susceptibility is

$$\chi = \frac{+\tilde{\mu}^2 \Delta N_o T_2}{\hbar} \left[\frac{T_2(\omega_{21} - \omega) - i}{1 + (\omega - \omega_{21})^2 T_2^2 + 4\Omega^2 T_2 \tau} \right]. \tag{A4}$$

Now Abrams and Lind (1) continue from this point and derive the scattering efficiency from the wave equation

$$\nabla^2 \vec{E} = \frac{\mu}{c^2} \frac{\partial^2 \vec{E}}{\partial t^2} + \frac{4\pi\mu}{c^2} \frac{\partial^2 \vec{P}}{\partial t^2} \tag{A5}$$

but ignores the angular dependence of the Laplacian operator. Using the geometry as defined in Figure 4, cylindrical geometry but ignoring the z dependence, the $\nabla^2 E$ term is

$$\nabla^2 \vec{E} = \frac{1}{r} \frac{\partial}{\partial r} \left(r \frac{\partial \vec{E}}{\partial r} \right) + \frac{1}{r^2} \frac{\partial^2 \vec{E}}{\partial \theta^2} \tag{A6}$$

The total electric field $\vec{E}$ is the sum of the fields from all four beams, i.e. Equations 11. Dropping the vector notation, time dependence, noting that $|K_1| = |K_2|$, and $|K_3| = |K_4|$, the electric field becomes

$$\begin{aligned} E(r) &= \frac{1}{2} A_1 e^{i\vec{K}_1 \cdot \vec{r}} + \frac{1}{2} A_2 e^{i\vec{K}_2 \cdot \vec{r}} + \frac{1}{2} A_3 e^{i\vec{K}_3 \cdot \vec{r}} + \frac{1}{2} A_4 E^{i\vec{K}_4 \cdot \vec{r}} + \text{c.c.} \\ &= \frac{1}{2} A_1 e^{-iK_1 r\cos\theta} + \frac{1}{2} A_2 e^{-ik_1 r\cos\theta} + \frac{1}{2} A_3 e^{iK_3 r\cos(\theta + \Delta)} + \\ &\frac{1}{2} A_4 e^{iK_3 r\cos(\theta + \Delta)} + \text{c.c.} \end{aligned} \tag{A7}$$

Applying the Laplacian operator to this field, the left hand side of the wave equation becomes

$$\nabla^2 E = \frac{1}{2}\frac{\partial}{\partial r}\left[\frac{\partial A_1}{\partial r} e^{-iK_1 r\cos\theta} + \frac{\partial A_2}{\partial r} e^{-iK_1 r\cos\theta} + \frac{\partial A_3}{\partial r} e^{iK_3 r\cos(\theta+\Delta)} + \right.$$

$$\frac{\partial A_4}{\partial r} e^{iK_3 r\cos(\theta+\Delta)} + (-iK_1\cos\theta)A_1 e^{-iK_1 r\cos\theta} +$$

$$(-iK_1\cos\theta)A_2 e^{-iK_1 r\cos\theta} + (iK_3\cos(\theta+\Delta))A_3 e^{iK_3 r\cos(\theta+\Delta)} +$$

$$\left.(iK_3\cos(\theta+\Delta))A_4 e^{iK_3 r\cos(\theta+\Delta)}\right] + \frac{1}{2r}\left[\frac{\partial A_1}{\partial r} e^{-iK_1 r\cos\theta} + \right.$$

$$\frac{\partial A_2}{\partial r} e^{-iK_1 r\cos\theta} + \frac{\partial A_3}{\partial r} e^{iK_3 r\cos(\theta+\Delta)} + \frac{\partial A_4}{\partial r} e^{iK_3 r\cos(\theta+\Delta)} +$$

$$(-iK_1\cos\theta)A_1 e^{-iK_1 r\cos\theta} + (-iK_1\cos\theta)A_2 e^{-iK_1 r\cos\theta} +$$

$$\left.(iK_3\cos(\theta+\Delta))A_3 e^{iK_3 r\cos(\theta+\Delta)} + (iK_3\cos(\theta+\Delta))e^{iK_3 r\cos(\theta+\Delta)}\right] +$$

$$\frac{1}{2r^2}\frac{\partial}{\partial\theta}\left[\frac{\partial A_1}{\partial\theta} e^{-iK_1 r\cos\theta} + \frac{\partial A_2}{\partial\theta} e^{-iK_1 r\cos\theta} + \frac{\partial A_3}{\partial\theta} e^{iK_3 r\cos(\theta+\Delta)} + \right.$$

$$\frac{\partial A_4}{\partial\theta} e^{iK_3 r\cos(\theta+\Delta)} + A_1(iK_1 r\sin\theta)e^{-iK_1 r\cos\theta} +$$

$$A_2(iK_1 r\sin\theta)e^{-iK_1 r\cos\theta} + A_3(-iK_3 r\sin(\theta+\Delta))e^{iK_3 r\cos(\theta+\Delta)} +$$

$$\left.A_4(-iK_3 r\sin(\theta+\Delta))e^{iK_3 r\cos(\theta+\Delta)}\right] \qquad \text{(A8)}$$

Carrying out the rest of the differentiation

$$\nabla^2 E = \frac{1}{2}\left[\frac{\partial^2 A_1}{\partial r^2} e^{-iK_1 r\cos\theta} + \frac{\partial^2 A_2}{\partial r^2} e^{-iK_1 r\cos\theta} + \frac{\partial^2 A_3}{\partial r^2} e^{iK_3 r\cos(\theta+\Delta)} + \right.$$

$$\frac{\partial^2 A_4}{\partial r^2} e^{iK_3 r\cos(\theta+\Delta)} + 2\frac{\partial A_1}{\partial r}(-iK_1\cos\theta)e^{-iK_1 r\cos\theta} +$$

$$2\frac{\partial A_2}{\partial r}(-iK_1\cos\theta)e^{-iK_1 r\cos\theta} + 2\frac{\partial A_3}{\partial r}(iK_3\cos(\theta+\Delta))e^{iK_3 r\cos(\theta+\Delta)} +$$

$$2\frac{\partial A_4}{\partial r}(iK_3\cos(\theta+\Delta))e^{iK_3r\cos(\theta+\Delta)} + (-iK_1\cos\theta)^2A_1e^{-iK_1r\cos\theta} +$$

$$(-iK_1\cos\theta)^2A_2e^{-iK_1r\cos\theta} + (iK_3\cos(\theta+\Delta))^2A_3e^{iK_3r\cos(\theta+\Delta)} +$$

$$(iK_3\cos(\theta+\Delta))^2A_4e^{iK_3r\cos(\theta+\Delta)}\Big] + \frac{1}{2r}\Big[\frac{\partial A_1}{\partial r}e^{-iK_1r\cos\theta} +$$

$$\frac{\partial A_2}{\partial r}e^{-iK_1r\cos\theta} + \frac{\partial A_3}{\partial r}e^{iK_3r\cos(\theta+\Delta)} + \frac{\partial A_4}{\partial r}e^{iK_3r\cos(\theta+\Delta)} +$$

$$(-iK_1\cos\theta)A_1e^{-iK_1r\cos\theta} + (-iK_1\cos\theta)A_2e^{-iK_1r\cos\theta} +$$

$$(iK_3\cos(\theta+\Delta))A_3e^{iK_3r\cos(\theta+\Delta)} + (iK_3\cos(\theta+\Delta))A_4e^{iK_3r\cos(\theta+\Delta)}\Big]$$

$$\frac{1}{2r^2}\Big[\frac{\partial^2A_1}{\partial\theta^2}e^{-iK_1r\cos\theta} + \frac{\partial^2A_2}{\partial\theta^2}e^{-iK_1r\cos\theta} + \frac{\partial^2A_3}{\partial\theta^2}e^{iK_3r\cos(\theta+\Delta)} +$$

$$\frac{\partial^2A_4}{\partial\theta^2}e^{iK_3r\cos(\theta+\Delta)} + 2\frac{\partial A_1}{\partial\theta}(iK_1r\sin\theta)e^{-ik_1r\cos\theta} +$$

$$2\frac{\partial A_2}{\partial\theta}(iK_1r\sin\theta)e^{-iK_1r\cos\theta} + 2\frac{\partial A_3}{\partial\theta}(-ik_3r\sin(\theta+\Delta))e^{iK_3r\cos(\theta+\Delta)} +$$

$$2\frac{\partial A_4}{\partial\theta}(-iK_3r\sin(\theta+\Delta))e^{iK_3r\cos(\theta+\Delta)} + A_1(iK_1r\sin\theta)^2e^{-iK_1r\cos\theta} +$$

$$A_2(iK_1r\sin\theta)^2e^{-iK_1r\cos\theta} + A_3(-iK_3r\sin(\theta+\Delta))^2e^{iK_3r\cos(\theta+\Delta)} +$$

$$A_4(-iK_3r\sin(\theta+\Delta))^2e^{iK_3r\cos(\theta+\Delta)} + A_1(iK_1r\cos\theta)e^{-iK_1r\cos\theta} +$$

$$A_2(iK_1r\cos\theta)e^{-iK_1r\cos\theta} + A_3(-iK_3r\cos(\theta+\Delta))e^{iK_3r\cos(\theta+\Delta)} +$$

$$A_4(-iK_3r\cos(\theta+\Delta))e^{iK_3r\cos(\theta+\Delta)}\Big] \qquad \text{(A9)}$$

Assuming the slowly varying envelope approximation,

$$\left|\frac{\partial^2 A_i}{\partial r^2}\right| << \left|K_i \frac{\partial A_i}{\partial r}\right| \text{ and } \frac{1}{r^2}\left|\frac{\partial^2 A_i}{\partial \theta^2}\right| << \frac{1}{r}\left|K_i \frac{\partial A_i}{\partial \theta}\right|,$$ the terms like $\frac{\partial^2 A_i}{\partial r^2}$ and $\frac{1}{r^2}\frac{\partial^2 A_i}{\partial \theta^2}$ can be neglected. The polarization can be simplified before it is substituted in the wave equation. Defining $\delta \equiv (\omega - \omega_{21})T_2$ as the detuning parameter, $\alpha_o \equiv \frac{\tilde{\mu}^2 \Delta N_o T_2}{\hbar}$ as the line center small-signal field attenuation coefficient, and $|E_s|^2 \equiv \frac{\hbar^2}{\tilde{\mu}^2 T_2 \tau}$ as the line center saturation intensity, the susceptibility becomes

$$\chi(E) = -\alpha_o\left[\frac{\delta + i}{1 + \delta^2 + \left|\frac{E}{E_s}\right|^2}\right] \tag{A10}$$

Using Equation 12 for the total electric field

$$\chi(E' + \Delta E) \simeq -\alpha_o(\delta + i)\left(1 + \delta^2 + \left|\frac{E'}{E_s}\right|^2 + \frac{E'^*\Delta E + \Delta E^* E'}{|E_s|^2}\right)^{-1} \tag{A11}$$

This can be simplified with a little algebra

$$\chi(E' + \Delta E) = \chi(E') - \chi(E')\left[\frac{E'^*\Delta E + \Delta E^* E'}{|E_s|^2}\right]\left(1 + \delta^2 + \left|\frac{E'}{E_s}\right|^2\right)^{-1} \tag{A12}$$

The polarization becomes

$$P(E) = \chi(E' + \Delta E)\left[E' + \Delta E\right] \tag{A13}$$

and after a little algebra

$$P(E) = \chi(E')\Delta E(1 + \delta^2)\left(1 + \delta^2 + \frac{|A_1|^2 + |A_3|^2}{|A_s|^2}\right)^{-1} +$$

$$\chi(E')E'\left[1 - \left(\frac{4E'\Delta E^*}{|A_s|^2}\right)\left(1 + \delta^2 + \frac{|A_1|^2 + |A_3|^2}{|A_s|^2}\right)^{-1}\right] \tag{A14}$$

where $|\vec{A}_1| = |\vec{A}_2|$ and $A_s = 2E_s$. Some of the necessary derivatives can be computed at this point

$$\frac{\partial^2}{\partial t^2}(\Delta E) = -\frac{1}{2}\left[\omega^2 A_2 e^{-i(\omega t + K_1 r\cos\theta)} + \omega'^2 A_4 e^{-i(\omega' t - K_3 r\cos(\theta + \Delta))}\right] \tag{A15}$$

and

$$\frac{\partial^2}{\partial t^2}(E') = -\frac{1}{2}\left[\omega^2 A_1 e^{-i(\omega t + K_1 r\cos\theta)} + \omega'^2 A_3 e^{-i(\omega' t - K_3 r\cos(\theta + \Delta))}\right] \tag{A16}$$

where ω' is the frequency of the read and signal beams and ω is the frequency of the write beams.

Now $E'^2 \Delta E^*$ needs to be computed. Being careful about keeping the complex conjugate terms (c.c.) in the field expressions, multiplying the fields together, and then separating the complex conjugate terms, the result is

$$E'^2 \Delta E^* = \frac{1}{8}\Bigg[A_1^2 A_2^* e^{-i(\omega t + K_1 r\cos\theta)} +$$

$$A_3^2 A_2^* e^{i([\omega - 2\omega']t + 2K_3 r\cos(\theta + \Delta) + K_1 r\cos\theta)} +$$

$$2A_1 A_3 A_2^* e^{-i(\omega' t - K_3 r\cos(\theta + \Delta))} + |A_1|^2 A_2^* e^{i(\omega t + K_1 r\cos\theta)} +$$

$$|A_3|^2 A_2^* e^{i(\omega t + K_1 r\cos\theta)} + 2A_1 A_3^* A_2^* e^{i(\omega' t - K_3 r\cos(\theta + \Delta))} +$$

$$A_1^2 A_4^* e^{-i([2\omega - \omega']t + 2K_1 r\cos\theta + K_3 r\cos(\theta + \Delta))} +$$

$$A_3^2 A_4^* e^{-i(\omega' t - K_3 r\cos(\theta + \Delta))} + 2A_1 A_3 A_4^* e^{-i(\omega t + K_1 r\cos\theta)} +$$

$$|A_1|^2 A_4^* e^{i(\omega' t - K_3 r\cos(\theta + \Delta))} + |A_3|^2 A_4^* e^{i(\omega' t - K_3 r\cos(\theta + \Delta))} +$$

$$2A_1^* A_3^* A_4^* e^{-i([\omega - 2\omega']t + K_1 r\cos\theta + 2K_3 r\cos(\theta + \Delta))} +$$

$$A_1^2 A_2 e^{-3i(\omega t + K_1 r\cos\theta)} + A_3^2 A_2 e^{-i([\omega + 2\omega']t - K_3 r\cos(\theta + \Delta) + K_1 r\cos\theta)}$$

$$2A_1 A_3 A_2 e^{-i([2\omega + \omega']t + 2K_1 r\cos\theta - K_3 r\cos(\theta + \Delta))} +$$

$$|A_1|^2 A_2 e^{-i(\omega t + K_1 r\cos\theta)} + A_2 |A_3|^2 e^{-i(\omega t + K_1 r\cos\theta)} +$$

$$2A_1 A_3^* A_2 e^{-i([2\omega - \omega']t + 2K_1 r\cos\theta + K_3 r\cos(\theta + \Delta))} +$$

$$A_1^2 A_4 e^{-i([2\omega + \omega']t + K_1 r\cos\theta - K_3 r\cos(\theta + \Delta))} +$$

$$A_3^2 A_4 e^{-3i(\omega' t - K_3 r\cos(\theta + \Delta))} +$$

$$2A_1 A_3 A_4 e^{-i([\omega + 2\omega']t + K_1 r\cos\theta - 2K_3 r\cos(\theta + \Delta))} +$$

$$|A_1|^2 A_4 e^{-i(\omega' t - K_3 r\cos(\theta + \Delta))} + |A_3|^2 A_4 e^{-i(\omega' t - K_3 r\cos(\theta + \Delta))} +$$

$$2A_1 A_3^* A_4 e^{-i(\omega t + K_1 r\cos\theta)} + \text{c.c.} \Bigg] \tag{A17}$$

Defining the complex modulation constant, which describes the coupling of the fields, and the complex refractive index constant, which describes saturated absorption and dispersion of the fields, as

$$(\Delta n)^* = \frac{2A_1^2}{|A_s|^2} \left[\frac{\alpha_o (i + \delta)}{\left(1 + \delta^2 + \dfrac{|A_1|^2 + |A_3|^2}{|A_s|^2}\right)^2} \right] \tag{A18}$$

$$n = \frac{-i\alpha_o (i + \delta)(1 + \delta^2)}{\left[1 + \delta^2 + \dfrac{|A_1|^2 + |A_3|^2}{|A_s|^2}\right]^2} \tag{A19}$$

where * denotes complex conjugation, and with the assumptions already made, without the time dependence and without the terms in $E'^2\Delta E^*$ whose phase oscillates at a frequency greater than phase of the fields alone, which would vanish upon averaging, the entire wave equation becomes

$$e^{i\vec{K}_1\cdot\vec{r}}\left[\frac{\partial A_1}{\partial r}\left(-\frac{1}{2r}-iK_1\cos\theta\right)+\frac{1}{r^2}\frac{\partial A_1}{\partial\theta}(iK_1 r\sin\theta)+\frac{1}{2}A_1(-iK_1\cos\theta)^2+\right.$$

$$\left.\frac{1}{2}A_1(iK_1\sin\theta)^2\right]+e^{i\vec{K}_2\cdot\vec{r}}\left[\frac{\partial A_2}{\partial r}\left(\frac{1}{2r}-iK_1\cos\theta\right)+\frac{1}{r^2}\frac{\partial A_2}{\partial\theta}(iK_1 r\sin\theta)+\right.$$

$$\left.\frac{1}{2}A_2(-iK_1\cos\theta)^2+\frac{1}{2}A_2(iK_1\sin\theta)^2\right]+e^{i\vec{K}_3\cdot\vec{r}}\left[\frac{\partial A_3}{\partial r}\left(-\frac{1}{2r}+iK_3\cos(\theta+\Delta)\right)+\right.$$

$$\frac{1}{r^2}\frac{\partial A_3}{\partial\theta}(-iK_3 r\sin(\theta+\Delta))+\frac{1}{2}A_3(iK_3\cos(\theta+\Delta))^2+$$

$$\left.\frac{1}{2}A_3(-iK_3\sin(\theta+\Delta))^2\right]+e^{i\vec{K}_4\cdot\vec{r}}\left[\frac{\partial A_4}{\partial r}\left(\frac{1}{2r}+iK_3\cos(\theta+\Delta)\right)+\right.$$

$$\frac{1}{r^2}\frac{\partial A_4}{\partial\theta}(-iK_3 r\sin(\theta+\Delta))+\frac{1}{2}A_4(iK_3\cos(\theta+\Delta))^2+$$

$$\left.\frac{1}{2}A_4(-iK_3\sin(\theta+\Delta))^2\right]=-\left(\frac{4\pi\mu}{c^2}\right)\left(\frac{\alpha_o}{2}\right)\left[\frac{i+\delta}{1+\delta^2+\frac{|A_1|^2+|A_3|^2}{|A_s|^2}}\right]$$

$$\left[\omega^2 A_2 e^{i\vec{K}_2\cdot\vec{r}}+\omega'^2 A_4 e^{i\vec{K}_4\cdot\vec{r}}\right]\left[\frac{1+\delta^2}{1+\delta^2+\frac{|A_1|^2+|A_3|^2}{|A_s|^2}}\right]$$

$$-\left(\frac{4\pi\mu}{c^2}\right)\left(\frac{\alpha_o}{2}\right)\left[\frac{i+\delta}{1+\delta^2+\frac{|A_1|^2+|A_3|^2}{|A_s|^2}}\right]\left[\omega^2 A_1 e^{i\vec{K}_1\cdot\vec{r}}+\omega'^2 A_3 e^{i\vec{K}_3\cdot\vec{r}}\right]+$$

$$\left(\frac{4\pi\mu}{c^2}\right)\left(\frac{\alpha_o}{2}\right)\left[\frac{i+\delta}{\left(1+\delta^2+\frac{|A_1|^2+|A_3|^2}{|A_s|^2}\right)}\right]^2\left(\frac{1}{|A_s|^2}\right)\Big\{\omega^2 A_1^2 A_2^* e^{i\vec{K}_1\cdot\vec{r}} +$$

$$2A_1A_3A_2^*\omega^2 e^{i\vec{K}_3\cdot\vec{r}} + \omega^2|A_1|^2A_2^* e^{-i\vec{K}_2\cdot\vec{r}} + \omega^2|A_3|^2A_2^* e^{-i\vec{K}_2\cdot\vec{r}} +$$

$$2A_1A_3^*A_2^*\omega^2 e^{-i\vec{K}_3\cdot\vec{r}} + \omega^2 A_3^2A_4^* e^{i\vec{K}_3\cdot\vec{r}} + 2\omega^2 A_1A_3A_4^* e^{i\vec{K}_1\cdot\vec{r}} +$$

$$|A_1|^2A_4^*\omega^2 e^{-i\vec{K}_4\cdot\vec{r}} + \omega^2|A_3|^2A_4^* e^{-i\vec{K}_4\cdot\vec{r}} + \omega^2|A_1|^2A_2 e^{i\vec{K}_2\cdot\vec{r}} +$$

$$|A_3|^2A_2\omega^2 e^{i\vec{K}_2\cdot\vec{r}} + \omega^2|A_1|^2A_4 e^{i\vec{K}_4\cdot\vec{r}} + \omega^2|A_3|^2A_4 e^{i\vec{K}_4\cdot\vec{r}} +$$

$$2\omega^2 A_1A_3^*A_4 e^{i\vec{K}_1\cdot\vec{r}}\Big\} + \frac{\mu}{c^2}\left[\left(\frac{-\omega^2}{2}\right)\left(A_1 e^{i\vec{K}_1\cdot\vec{r}} + A_2 e^{i\vec{K}_2\cdot\vec{r}} + \right)\right.$$

$$\left.\left(\frac{-\omega^2}{2}\right)\left(A_3 e^{i\vec{K}_3\cdot\vec{r}} + A_4 e^{i\vec{K}_4\cdot\vec{r}}\right)\right] + [\text{c.c. terms on both sides of}$$

the equation] . (A20)

This equation must be true for all angles, θ. Thus all of the terms with the same exponential factors must be equal independently. The FWM scattering efficiency, η, is proportional to the power reflection coefficient or reflectivity, R,

$$\eta = \frac{I_2}{I_3} R \tag{A21}$$

where $R \equiv \frac{I_4}{I_2}$, and I_i (i = 1,2,3,4) is the intensity of each beam. The only terms that need be kept in the wave equation in order to calculate R are the A_2 and A_4 terms. Making an assumption at this point that is true for degenerate FWM, but is only an approximation in this case

$$\vec{K}_2 = -\vec{K}_4 \text{ and } \vec{K}_1 = -\vec{K}_3 \tag{A22}$$

the equations become

$$\frac{\partial A_2}{\partial r}\left(\frac{1}{2r} - iK_1\cos\theta\right) + \frac{\partial A_2}{\partial \theta}\left(\frac{iK_1}{r}\sin\theta\right) - A_2\left(\frac{1}{2}K_1^2\right) + \left(\frac{\mu\omega^2}{2c^2}\right)A_2 =$$

$$\left(\frac{-2\pi\mu\omega^2 in}{c^2}\right)A_2 + \frac{2\pi\mu}{c^2|A_1|^2}\left(\frac{\Delta n^*}{2}\right)\left\{A_2\omega^2\left[|A_1|^2 + |A_3|^2\right] + A_4^*\omega^2\left[|A_1|^2 + |A_3|^2\right]\right\} \quad \text{(A23)}$$

$$\frac{\partial A_4}{\partial r}\left(\frac{1}{2r} + iK_3\cos(\theta + \Delta)\right) - \frac{\partial A_4}{\partial \theta}\left(\frac{iK_3}{r}\sin(\theta + \Delta)\right) - A_4\left(\frac{1}{2}K_3^2\right) + \left(\frac{\mu\omega^2}{2c^2}\right)A_4 =$$

$$\left(\frac{-2\pi\mu\omega^2 in}{c^2}\right)A_4 + \frac{2\pi\mu}{c^2|A_1|^2}\left(\frac{\Delta n^*}{2}\right)\left\{A_4\omega^2\left[|A_1|^2 + |A_3|^2\right] + A_2^*\omega^2\left[|A_1|^2 + |A_3|^2\right]\right\} \quad \text{(A24)}$$

Making the assumption that there is no beam depletion for the signal beam and write beams $\left[\frac{\partial A_2}{\partial r}, \frac{\partial A_4}{\partial r} << 1\right]$, and that the write beams are much more intense than the read beam $|A_3|^2 << |A_1|^2$, equations (A23-A24) become

$$\frac{\partial A_2}{\partial \theta}\left(\frac{iK_1}{r}\sin\theta\right) + A_2\left[\frac{\mu\omega^2}{2c^2} - \frac{1}{2}K_1^2 + \frac{2\pi\mu\omega^2 in}{c^2} - \frac{\pi\omega^2\mu\Delta n^*}{c^2}\right] =$$

$$\frac{\pi\omega^2\mu}{c^2}(\Delta n)^* A_4^* \quad \text{(A25)}$$

$$\frac{\partial A_4}{\partial \theta}\left(\frac{-iK_3}{r}\sin(\theta + \Delta)\right) + A_4\left[\frac{\mu\omega^2}{2c^2} - \frac{1}{2}K_3^2 + \frac{2\pi\mu\omega^2 in}{c^2} - \frac{\pi\omega^2\mu\Delta n^*}{c^2}\right] = \frac{\pi\omega^2\mu}{c^2}(\Delta n)^* A_2^* \quad \text{(A26)}$$

Changing variables to $\Theta = \theta + \Delta$ in Equation (A26) and eliminating the complex nature of these two equations by equating the real and imaginary parts of each equation.

$$\frac{\partial A_2^{\,i}}{\partial \theta} = \frac{r}{c^2 K_1}\left\{\omega^2\left[A_2^{\,r}C_1^{\,r} - A_2^{\,i}C_1^{\,i} - A_2^{\,r}C_2^{\,r} - A_2^{\,i}C_2^{\,i}\right]\csc\theta - \omega^{-2}\left[C_2^{\,r}A_4^{\,r} - C_2^{\,i}A_4^{\,i}\right]\csc\theta\right\} \tag{A27}$$

$$\frac{\partial A_2^{\,r}}{\partial \theta} = \frac{r}{c^2 K_1}\left\{\omega^2\left[-A_2^{\,i}C_1^{\,r} - A_2^{\,r}C_1^{\,i} + A_2^{\,i}C_2^{\,r} - A_2^{\,r}C_2^{\,i}\right]\csc\theta - \omega^{-2}\left[C_2^{\,i}A_4^{\,r} + C_2^{\,r}A_4^{\,i}\right]\csc\theta\right\} \tag{A28}$$

$$\frac{\partial A_4^{\,i}}{\partial \theta} = \frac{r}{c^2 K_3}\left\{\omega^{-2}\left[-A_4^{\,r}C_1^{\,r} + A_4^{\,i}C_1^{\,i} + A_4^{\,r}C_2^{\,r} + A_4^{\,i}C_2^{\,i}\right]\csc\theta + \omega^2\left[C_2^{\,r}A_2^{\,r} - C_2^{\,i}A_4^{\,i}\right]\csc\theta\right\} \tag{A29}$$

$$\frac{\partial A_4^{\,r}}{\partial \theta} = \frac{r}{c^2 K_3}\left\{\omega^{-2}\left[A_4^{\,i}C_1^{\,r} + A_4^{\,r}C_1^{\,i} - A_4^{\,i}C_2^{\,r} + A_4^{\,r}C_2^{\,i}\right]\csc\theta + \omega^2\left[C_2^{\,r}A_2^{\,i} + C_2^{\,i}A_2^{\,r}\right]\csc\theta\right\} \tag{A30}$$

where $C_1 \simeq 2\pi\mu i n$ and $C_2^{\,*} = \pi\mu(\Delta n)^*$, and the superscripts r and i stand for real and imaginary, respectively. Incorporating r in the constants C_1 and C_2, these equations become

$$\frac{\partial A_2^{\,i}}{\partial \theta} = \left\{\left[A_2^{\,r}D_1^{\,r} - A_2^{\,i}D_1^{\,i} - A_2^{\,r}D_2^{\,r} - A_2^{\,i}D_2^{\,i}\right]K_1\csc - \left[D_2^{\,r}A_4^{\,r} - D_2^{\,i}A_4^{\,i}\right]\frac{K_3^{\,2}}{K_1}\csc\theta\right\} \tag{A31}$$

$$\frac{\partial A_2^r}{\partial\theta}\left\{\left[-A_2^i D_1^r - A_2^r D_1^i + A_2^i D_2^r - A_2^r D_2^i\right] K_1 \csc\theta - \left[D_2^i A_4^r + D_2^r A_4^i\right] \frac{K_3^2}{K_1} \csc\theta\right\} \tag{A32}$$

$$\frac{\partial A_4^i}{\partial\theta} = \left\{\left[-A_4^r D_1^r + A_4^i D_1^i + A_4^r D_2^r + A_4^i D_2^i\right] K_3 \csc\theta + \left[D_2^r A_2^r - D_2^i A_2^i\right] \frac{K_1^2}{K_3} \cos\theta\right\} \tag{A33}$$

$$\frac{\partial A_4^r}{\partial\theta} = \left\{\left[A_4^i D_1^r + A_4^r D_1^i - A_4^i D_2^r + A_4^r D_2^i\right] K_3 \csc\theta + \left[D_2^r A_2^i + D_2^i A_2^r\right] \frac{K_1^2}{K_3} \cos\theta\right\} \tag{A34}$$

where $D_1^r = rC_1^r$, $D_1^i = rC_1^i$, $D_2^r = rC_2^r$, and $D_2^i = rC_2^i$. These four equations must be solved in order to find the angular dependence of the absolute scattering efficiency, which is defined as

$$\eta = \frac{|A_4|^2}{|A_3|^2} \tag{A35}$$

and is related to the power reflection coefficient by

$$\eta = \left(\frac{|A_2|^2}{|A_3|^2}\right) R = \left(\frac{|A_2|^2}{|A_3|^2}\right)\left(\frac{|A_4^{r2}| + |A_4^{i2}|}{|A_2^{r2}| + |A_2^{i2}|}\right) \tag{A36}$$

The proportionality factor $\frac{I_2}{I_3} = \frac{|A_2|^2}{|A_3|^2}$ is just a constant since $I_1 = I_2$, $I_3 >> I_4$ where I_i (i = 1,2,3,4) is the beam intensity, i.e. there is negligible beam depletion and the absolute scattering efficiency is much less than 1. Since the scattering efficiency is normalized in the measurements taken the normalized scattering efficiency can be

defined as follows (5)

$$\eta = A_4 A_4^* = \left| A_4^{r^2} + A_4^{i^2} \right| \tag{A37}$$

VITA

Guy Donald Gilliland

Candidate for the Degree of

Master of Science

Thesis: OPTICAL SPECTROSCOPY OF ALEXANDRITE CRYSTALS

Major Field: Physics

Biographical:

Personal Data: Born in Dallas, Texas, August 16, 1962, the son of Donald C. and Janis G. Gilliland. Married to Marcia Ann Murphy on June 29, 1985.

Education: Graduated from Putnam City North High School, Oklahoma City, Oklahoma, in May, 1980; received the Bachelor of Science degree from Baylor University in May, 1984, with a major in Physics and a minor in German; completed the requirements for the Master of Science degree at Oklahoma State University in May, 1986.

Professional Experience: Undergraduate Research Assistant, Oklahoma State University, May, 1983 to August, 1983; Graduate Teaching Assistant, Oklahoma State University, August, 1984 to December, 1984; Graduate Research Assistant, Oklahoma State University, January, 1985 to present; Office of Naval Research Graduate Fellow, September, 1984 to September, 1984; Member of the American Physical Society and the Optical Society of America.